Hydrol. Earth Syst. Sci. Discuss., doi:10.5194/hess-2015-552, 2016
Manuscript under review for journal Hydrol. Earth Syst. Sci.
Published: 27 January 2016

Hydrology and Earth System Sciences
Open Access
Discussions

Canopy-scale biophysical controls of transpiration and evaporation in the Amazon Basin

Kaniska Mallick[1], Ivonne Trebs[1], Eva Boegh[2], Laura Giustarini[1], Martin Schlerf[1], Darren Drewry[3], Lucien Hoffmann[1], Celso von Randow[4], Bart Kruijt[5], Alessandro Araùjo[6], Scott Saleska[7], James R. Ehleringer[8], Tomas F. Domingues[9], Jean Pierre H. B. Ometto[4], Antonio D. Nobre[4], Osvaldo Luiz Leal de Moraes[10], Matthew Hayek[11], J. William Munger[11], Steve Wofsy[11]

[1]Department of Environmental Research and Innovation, Luxembourg Institute of Science and Technology (LIST), Belvaux, Luxembourg

[2]Department of Environmental, Social and Spatial Change, Roskilde University, Roskilde, Denmark

[3]Jet Propulsion Laboratory, California Institute of Technology, 4800 Oak Grove Drive, Pasadena, 91109, USA

[4]Instituto Nacional de Pesquisas Espaciais (INPE), Centro de Ciência do Sistema Terrestre, São José dos Campos, SP, Brazil

[5]Alterra, Wageningen University and Research Centre, Wageningen, The Netherlands

[6]Empresa Brasileira de Pesquisa Agropecuária (EMBRAPA), Belém-PA, Brazil

[7]Department of Ecology and Evolutionary Biology, University of Arizona, Tucson, AZ, USA

[8]Department of Biology, University of Utah, Salt Lake City, UT, USA

[9]Faculdade de Filosofia Ciências e Letras de Ribeirão Preto, Universidade de São Paulo (USP), São Paulo, SP, Brazil

[10]Centro Nacional de Monitoramento e Alertas de Desastres Naturais, SP-RJ, Brazil

[11]Harvard University, Cambridge, MA, USA

Corresponding Authors: Kaniska Mallick (Phone: +352 275888425; Email: kaniska.mallick@gmail.com); Ivonne Trebs **(**Phone: +352 275888880; Email: ivonne.trebs@list.lu**)**

Running head:

Bio-physical controls on evapotranspiration

Hydrol. Earth Syst. Sci. Discuss., doi:10.5194/hess-2015-552, 2016
Manuscript under review for journal Hydrol. Earth Syst. Sci.
Published: 27 January 2016

Hydrology and Earth System Sciences
Open Access
Discussions

Abstract:

Canopy and aerodynamic conductances (g_C and g_A) are some of the key land surface variables determining the land surface response of climate models. Their representation is crucial for predicting transpiration (λE_T) and evaporation (λE_E), which has important implications for global climate change and water resource management. Here, we present a novel approach to directly quantify the controls of the canopy-scale conductances on λE_T and λE_E over multiple plant functions types (PFTs) in the Amazon Basin. Combining data from six LBA (Large-scale Biosphere-Atmosphere Experiment in Amazonia) eddy covariance tower sites and a physically-based modeling approach, we identified the canopy-scale feedback-response mechanism between g_C, λE_T, and atmospheric vapor pressure deficit (D_A), which was originally postulated to occur at the leaf-scale. We show minor biophysical control on λE_T under wet conditions where net radiation (R_N) determines 75% to 80% of the variances of λE_T. However, biophysical control on λE_T is amplified during the drought year (2005) and dry conditions, explaining 50% to 65% of the variances of λE_T. Despite substantial differences in g_A, nearly similar 'coupling' was found in forests and pastures due to the increase of g_C induced by soil moisture. This suggests that the relative response of g_C to per unit change of wetness is significantly higher compared to g_A. Our results reveal the occurrence of a larger magnitude of hysteresis between λE_T and g_C during the dry season for the pasture sites, which is attributed to relatively low soil water availability compared to the rainforest. Evaporation was significantly influenced by g_A for all the PFTs and across all wetness conditions. Our analytical framework faithfully captures the responses of g_C and g_A to changing atmospheric radiation, D_A, and surface skin temperature, and, thus appears to be promising for the improvement of existing land surface parameterisations at a range of spatial scales.

Hydrol. Earth Syst. Sci. Discuss., doi:10.5194/hess-2015-552, 2016
Manuscript under review for journal Hydrol. Earth Syst. Sci.
Published: 27 January 2016

Keywords: Canopy conductance, aerodynamic conductance, transpiration, evaporation, Penman-Monteith, Shuttleworth-Wallace, coupling, Amazon, LBA

Hydrol. Earth Syst. Sci. Discuss., doi:10.5194/hess-2015-552, 2016
Manuscript under review for journal Hydrol. Earth Syst. Sci.
Published: 27 January 2016

Hydrology and Earth System Sciences
Discussions
Open Access
EGU

1 Introduction

The Amazon rainforest is one of the world's most extensive natural ecosystems influencing the Earth's water, energy, and carbon cycles (Malhi et al., 2012), and also a major source of global terrestrial evapotranspiration (E) or latent heat flux (λE) (Costa et al., 2010; Harper et al., 2014). An intensification of the Amazon hydrological cycle was observed in the past two decades characterised by increased temperatures and more frequent droughts and floods (Cox et al., 2000; Huntingford et al., 2008; Gloor et al., 2013). Recent Amazonian droughts have gained particular attention due to the sensitivity of the tropical forest λE to climate change (Hilker et al., 2014). A very recent study suggests that, in case of persistent precipitation extremes (Hilker et al., 2014), the Amazon forest may become an increasing carbon source as a result of both the suppression of net biome exchange by drought and emissions from fires (Gatti et al., 2014). Moreover, changes in land cover due to conversion of tropical forest to pastures significantly alters the energy partitioning by decreasing λE and increasing sensible heat fluxes (H) over pasture sites (e.g. Priante-Filho et al., 2004). This will ultimately lead to severe consequences for the water balance in the region, with increased (or decreased) river discharge already prevailing in some parts of the Basin (Davidson et al., 2012). Evaluating the λE response to changing climate and land use in the Amazon basin is critical to understand the stability of the tropics within the Earth system (Lawrence and Vandecar, 2015). Therefore, quantifying the critical role of biophysical variables on λE will add substantial insight to assess the resilience of Amazon basin under global change.

The aerodynamic and canopy conductances (g_A and g_C, hereafter) (unit m s^{-1}) are two most important biophysical (biological + physical) variables regulating the evaporation (λE_E) and transpiration (λE_T) components of λE (Monteith and Unsworth, 2008; Dolman et al., 2014; Raupach, 1995; Colaizzi et al., 2012; Bonan et al., 2014). While g_A controls the bulk aerodynamic transfer of energy and water through the near-surface boundary layer, g_C

Hydrol. Earth Syst. Sci. Discuss., doi:10.5194/hess-2015-552, 2016
Manuscript under review for journal Hydrol. Earth Syst. Sci.
Published: 27 January 2016

Hydrology and Earth System Sciences
Discussions

represents the restriction on water vapour flow through the aggregated conductance from stomata of the leaves in case of vegetation. In case of partial vegetation cover g_C also includes evaporation from soil surface. The Penman-Monteith (PM) equation is a physically-based scheme for quantifying the biophysical controls on canopy-scale λE_E and λE_T from terrestrial ecosystems, treating the vegetation canopy as a 'big-leaf' (Monteith, 1965; 1981). Despite its development based on biophysical principles controlling water vapour exchange, quantifying the g_A and g_C controls on λE through the PM equation suffers from the continued longstanding uncertainty over the aggregated stomatal and aerodynamic behaviour within the soil-plant-atmosphere-continuum (Matheny et al., 2014; Prihodko et al., 2008).

One of the major sources of uncertainties in modeling g_A is associated with the empirical (and uncertain) parameterizations of near-surface boundary layer dynamics, which is invariably confounded by space-time variability in atmospheric stability (van der Tol et al., 2009; Shuttleworth, 1989). For example, Monin-Obukhov Similarity Theory (MOST) appears to be only be valid over uniform, extensive, and flat surfaces (Monteith and Unsworth, 2008; van der Tol et al., 2009; Holwerda et al., 2012), and its application to complex 'real' canopy systems is problematic due to chaotic interactions between turbulence, canopy roughness and topography (Raupach and Finnigan, 1995; Shuttleworth, 2007; Holwerda et al., 2012). Similarly, g_C varies in space and time due to variations in plant species, photosynthetic capacity, soil moisture variability and environmental drivers (Monteith and Unsworth, 2008; van der Tol et al., 2009). Despite the existence of several semi-mechanistic and empirical parameterisations for g_C (e.g. Ball et al., 1987; Leuning, 1995; Tuzet et al., 2003; Medlyn et al., 2011), the adaptive tendencies of plant canopies severely compromises the efficacy of such approaches (Matheny et al., 2014), limiting their applicability over most landscapes. Thus, debate over the most appropriate model of canopy conductance has endured for decades.

Hydrol. Earth Syst. Sci. Discuss., doi:10.5194/hess-2015-552, 2016
Manuscript under review for journal Hydrol. Earth Syst. Sci.
Published: 27 January 2016

Previous studies in the Amazon Basin focussed on observational understanding of biogeochemical cycling of energy, water, carbon, trace gases, and aerosols in Amazonia (Andreae et al., 2002; Malhi et al., 2002; da Rocha et al., 2009), model-based understanding of surface ecophysiological behaviour and seasonality of λE (Baker et al., 2013; Christoffersen et al., 2014), modelling the controls on λE (Hasler and Avissar, 2007; Costa et al., 2010), understanding seasonality of photosynthesis and of λE (da Rocha et al., 2004; Restrepo-Coupe et al., 2013) and the impact of land use on hydrometeorology (Roy and Avissar, 2002; von Randow et al., 2012). However, the combination of climatic and ecohydrological disturbances will significantly affect the stomatal functioning, the partitioning of λE_E-λE_T and carbon-water-climate interactions of the tropical vegetation (Cox et al., 2000; Mercado et al., 2009). Hence, investigation of the effects of drought and land cover changes on conductances, λE_E, and λE_T is a topic requiring urgent attention (Blyth et al., 2010) both because of the cursory way it is handled in current generation parametric models (Matheny et al., 2014) and because of the importance of the response of g_A and g_C in controlling the model behaviour (Villagarcía et al., 2010). Given the persistent risk of deforestation, the ecophysiological changes of different plant functional types (PFTs) are expected to be reflected in g_A and g_C and λE_E and λE_T. Besides inverting the PM equation using field measurements of λE, up to date only leaf-scale experiments were performed to directly quantify g_C (Meinzer et al., 1993, 1997; Monteith, 1995; Jones, 1998; Motzer et al., 2005). However, an analytical or physical retrieval for g_A and g_C required to understand the role of the canopy in regulating evaporation and transpiration of water is still lacking. This paper aims to leverage this emerging opportunity by exploring data from the Large-scale Biosphere-Atmosphere Experiment in Amazonia (LBA) eddy covariance (EC) observations (e.g., de Gonçalves et al., 2013; Restrepo-Coupe et al., 2013) using a novel analytical modeling technique, the Surface Temperature Initiated Closure (STIC) (STIC1.0 and

Hydrol. Earth Syst. Sci. Discuss., doi:10.5194/hess-2015-552, 2016
Manuscript under review for journal Hydrol. Earth Syst. Sci.
Published: 27 January 2016

STIC1.1) (Mallick et al., 2014, 2015) in order to quantify the biophysical control on λE_E and λE_T over several representative PFTs of the Amazon Basin.

STIC provides a framework for simultaneously retrieving g_A and g_C, and surface energy balance fluxes. It is based on finding analytical solutions for g_A and g_C by physically integrating radiometric surface temperature (T_R) information (along with radiative fluxes, meteorological variables) into the PM model (Mallick et al., 2014, 2015). The direct estimates of canopy-scale conductances and λE obtained through STIC are independent of any land surface parameterisation. *This contrasts with the multi-layer canopy models that explicitly parameterize the leaf-scale conductances and perform bottom-up scaling to derive the canopy-scale conductances (Baldocchi et al., 2002; Drewry et al., 2010).*

This study addresses the following science questions and objectives:

(1) How realistic are the canopy-scale conductances and their behaviour when estimated analytically (or non-parametrically) without involving any empirical land surface parameterization?

(2) What are the controls of canopy-scale g_A and g_C on evaporation and transpiration in the Amazon basin?

(3) How do the STIC-based canopy-scale conductances compare with known (or believed) environmental constraints?

(4) Is the biological response of g_C consistent with the leaf-scale theory (Jarvis and McNaughton, 1986; McNaughton and Jarvis, 1991; Monteith, 1995)?

The following section describes a brief methodology to retrieve g_C, g_A, λE_E, and λE_T. The data sources used for the analysis are described after the methodology and will be followed by a comparison of the results with fluxes derived from EC measurements. A detailed

Hydrol. Earth Syst. Sci. Discuss., doi:10.5194/hess-2015-552, 2016
Manuscript under review for journal Hydrol. Earth Syst. Sci.
Published: 27 January 2016

Hydrology and Earth System Sciences
Discussions

discussion of the results and potential applicability of the method with implications for global change research are elaborated at the end.

2 Methodology

2.1 Theory

The retrieval of g_A, g_C, and λE are based on finding a 'closure' of the PM equation (eq. 1 below) using the STIC framework (Fig. A1) (Mallick et al., 2015). STIC is a physically-based single-source surface energy balance scheme which includes internally consistent estimation of g_A and g_C (Mallick et al., 2014, 2015). Originally designed for application to thermal remote sensing data from Earth observation sensors, the STIC framework exploits observations of T_R, radiative, and environmental variables including net radiation (R_N), ground heat flux (G), air temperature (T_A), relative humidity (R_H) or vapor pressure (e_A) at a reference level above the surface.

The PM equation is commonly expressed as,

$$\lambda E = \frac{s\phi + \rho c_P g_A D_A}{s + \gamma\left(1 + \frac{g_A}{g_C}\right)} \quad (1)$$

where ρ is the air density (kg m^{-3}), c_P is the specific heat of air (J kg^{-1} K^{-1}), γ is the psychrometric constant (hPa K^{-1}), s is the slope of the saturation vapor pressure versus air temperature (hPa K^{-1}), D_A is the saturation deficit of the air (hPa) or vapor pressure deficit at the reference level, and ϕ is the net available energy (W m^{-2}) (the difference between R_N and G). The units of all the surface fluxes and conductances are in W m^{-2} and m s^{-1}, respectively. Traditionally, the two unknowns in eq. 1 are g_A and g_C. Therefore, the STIC methodology is based on formulating state equations (eq. 2 to 5 below) for these conductances that satisfy the PM equation (for detailed derivations of eq. 2 to 5 see Mallick et al., 2014, 2015).

Hydrol. Earth Syst. Sci. Discuss., doi:10.5194/hess-2015-552, 2016
Manuscript under review for journal Hydrol. Earth Syst. Sci.
Published: 27 January 2016

Hydrology and Earth System Sciences
Discussions

$$g_A = \frac{\phi}{\rho c_P \left[(T_o - T_A) + \left(\frac{e_0 - e_A}{\gamma}\right)\right]} \quad (2)$$

$$g_C = g_A \frac{(e_0 - e_A)}{(e_0^* - e_0)} \quad (3)$$

$$T_o = T_A + \left(\frac{e_0 - e_A}{\gamma}\right)\left(\frac{1 - \Lambda}{\Lambda}\right) \quad (4)$$

$$\Lambda = \frac{2\alpha s}{2s + 2\gamma + \gamma \frac{g_A}{g_C}(1 + M)} \quad (5)$$

196 Here, T_0 is the temperature (°C) at the source/sink height (or at the roughness length (z_0) or
197 in-canopy air stream), e_0 is the atmospheric vapor pressure (hPa) at the source/sink height, e_0^*
198 is the saturation vapor pressure (hPa) at the source/sink height, Λ is the evaporative fraction
199 (the ratio of λE and ϕ), α is the Priestley-Taylor parameter (unitless) (Priestley and Taylor,
200 1972), and M is a unitless quantity which describes the relative wetness of the surface. M
201 controls the transition from potential to actual evaporation and hence is critical for providing
202 the constraint against which the conductances can be estimated. Given the information of R_N,
203 G, T_A, R_H or e_A, and T_R, these state equations can be solved simultaneously to derive
204 analytical solutions for g_A and g_C. This also produces a 'closure' of the PM model, which is
205 independent of empirical parameterizations for both g_A and g_C. The analytical solution to the
206 state equations 2-5 have three additional unknowns; e_0^*, e_0, and α, and these variables are
207 iteratively estimated as described in the Appendix, which is also a modification of the
208 STIC1.1 framework (Mallick et al., 2015). The present version of STIC is designated as
209 STIC1.2. STIC uses T_R as an additional data source to retrieve M and the estimation of M is
210 also explained in the Appendix. The detailed derivations of the state equations (eq. 2 to 5) of
211 STIC are described in Mallick et al. (2014; 2015).

212 **2.2 Partitioning λE**

213 The terrestrial latent heat flux is an aggregate of both transpiration (λE_T) and evaporation
214 (λE_E) (sum of soil evaporation and interception evaporation from canopy). During rain events

Hydrol. Earth Syst. Sci. Discuss., doi:10.5194/hess-2015-552, 2016
Manuscript under review for journal Hydrol. Earth Syst. Sci.
Published: 27 January 2016

the land surface becomes wet and λE tends to approach the potential evaporation (λE^*), while surface drying after rainfall causes λE to approach the potential transpiration rate (λE_T^*) in the presence of vegetation, or zero without any vegetation. Hence, λE at any time is a mixture of these two end member conditions depending on the degree of surface moisture availability or wetness (M) (Bosveld and Bouten, 2003; Loescher et al., 2005). Considering the general case of evaporation from any nonsaturated surface at a rate less than the potential, M is the ratio of the actual to the potential evaporation rate and is considered as an index of evaporation efficiency during a given time interval (Boulet et al., 2015). Partitioning of λE into λE_E and λE_T was performed according to Mallick et al. (2014) as follows:

$$\lambda E = \lambda E_E + \lambda E_T = M\lambda E^* + (1-M)\lambda E_T^* \qquad (6)$$

The estimates of λE_E in the current method consists of aggregated contribution from both interception and soil evaporation, and no further attempt is made to separate these two components. After estimating g_A, λE^* was estimated according to the Penman equation and λE_T was estimated as the residual in equation 6.

In this study, we use the term 'canopy conductance' instead of 'stomatal conductance' given the term 'stomata' is applicable at the leaf-scale only. It is important to appreciate that g_C should principally be a mixture of the stomatal (or biological) and soil conductances. However, given the high vegetation density of the Amazon Basin, the soil surface exposure is negligible, and, hence we assume g_C to be the canopy-scale aggregate of stomatal conductance.

2.3 Evaluating g_A and g_C

Due to the lack of direct canopy-scale g_A measurements, a rigorous evaluation of g_A cannot be performed. To evaluate the STIC retrievals of g_A ($g_{A\text{-}STIC}$) we adopted three different methods:

Hydrol. Earth Syst. Sci. Discuss., doi:10.5194/hess-2015-552, 2016
Manuscript under review for journal Hydrol. Earth Syst. Sci.
Published: 27 January 2016

(a) By exploring the measured friction velocity (u^*) and wind speed (u) at the EC towers and using the equation of Baldocchi and Ma (2013) ($g_{A\text{-}BM13}$) in which g_A was expressed as sum of turbulent conductance and canopy (quasi-laminar) boundary layer conductance as,

$$g_{A\text{-}BM13} = [(u/u^{*2}) + (2/ku^{*2})(S_c/P_r)^{0.67}]^{-1} \quad (7)$$

where k is von Karman's constant, 0.4; S_c is the Schmidt Number; P_r is the Prandtl Number and their ratio is generally considered to be unity.

(b) By inverting λE observations for wet conditions hence assuming $\lambda E \cong \lambda E^*$ and estimating g_A ($g_{A\text{-}INV}$) as,

$$g_{A\text{-}INV} = \gamma\lambda E/\rho c_P D_A \quad (8)$$

(c) By inverting the aerodynamic equation of H and estimating a hybrid g_A ($g_{A\text{-}HYB}$) from observed H and STIC T_0 as ($T_{0\text{-}STIC}$),

$$g_{A\text{-}HYB} = H/\rho c_P(T_{0\text{-}STIC} - T_A) \quad (9)$$

Similarly, we compared the STIC derived g_C ($g_{C\text{-}STIC}$) with g_C estimated by inverting the PM model ($g_{C\text{-}INV}$) (Monteith, 1995) exploiting $g_{A\text{-}BM13}$ in conjunction with the available ϕ, λE, T_A, and D_A measurements from the EC towers.

3 Datasets

3.1 Eddy covariance and meteorological quantities

We have used the LBA (Large-Scale Biosphere-Atmosphere Experiment in Amazonia) data for quantifying the biophysical controls on the evaporative flux components. LBA is an international research initiative conducted from 1995-2005 to study how Amazonia functions as a regional entity within the larger Earth system, and how changes in land use and climate will affect the hydrological and biogeochemical functioning of the Amazon ecosystem (Andreae et al., 2002).

Hydrol. Earth Syst. Sci. Discuss., doi:10.5194/hess-2015-552, 2016
Manuscript under review for journal Hydrol. Earth Syst. Sci.
Published: 27 January 2016

Hydrology and Earth System Sciences
Discussions

A network of eddy covariance (EC) towers was operational during the LBA experiment, such that data from nine EC towers were obtained from the ORNL Distributed Archive Active Centre (ftp://daac.ornl.gov/data/lba/carbon_dynamics/CD32_Brazil_Flux_Network/). These are the quality controlled and harmonized surface flux and meteorological data from the Brazilian Amazon flux network. Time series of surface fluxes (λE, H, G), radiation (T_R, R_N, shortwave and longwave), meteorological quantities (T_A, R_H, wind speed) as well as soil moisture and rainfall were available from six (out of nine) EC towers. Three of the EC towers had numerous missing data and were not included in the analysis. The surface energy balance was closed by applying the Bowen ratio (Bowen, 1926) closure as described in Chavez et al. (2005) and later adopted by Anderson et al. (2007) and Mallick et al. (2015). In the absence of G measurements, ϕ was assumed to be equal to the sum of λE and H. For the present analysis, data from six EC towers (Table 1) were selected, which represent two different biomes (forest and pasture) covering four different PFTs, namely, tropical rainforest (TRF), tropical moist forest (TMF), tropical dry forest (TDF), and pasture (PAS), respectively. A general description of the datasets can be found in Saleska et al. (2013). For all sites, monthly averages of the diurnal cycle (hourly time resolution) were chosen for the present analysis.

4 Results

4.1 Evaluating g_A, g_C and surface energy balance fluxes

Examples of monthly averages of the diurnal cycles of the four different g_A estimates and their corresponding g_C estimates over two different PFTs (K34 for forest and FNS for pasture) reveal that $g_{A\text{-}STIC}$ and $g_{C\text{-}STIC}$ tend to be generally higher over the forest than their counterparts, varying from 0 to 0.06 m s^{-1} and 0 to 0.04 m s^{-1} respectively (Fig. 1a and 1b). The magnitude of $g_{A\text{-}STIC}$ varied between 0 to 0.025 m s^{-1} for the pasture (Fig. 1a), while $g_{C\text{-}STIC}$ values were less than half that of those estimated over the forest (0 – 0.01 m s^{-1}) (Fig. 1b). The conductances showed a marked diurnal variation expressing their overall dependence on

Hydrol. Earth Syst. Sci. Discuss., doi:10.5194/hess-2015-552, 2016
Manuscript under review for journal Hydrol. Earth Syst. Sci.
Published: 27 January 2016

net radiation, vapor pressure deficit, and surface temperature. Despite the absolute differences between the conductances from the different retrieval methods, their diurnal patterns were comparable.

The canopy-scale evaluation of $g_{A\text{-}STIC}$ is illustrated in Fig. 2a (and Table 2) combining data from the four PFTs. Estimated values range between zero and 0.1 m s^{-1} and show modest correlation (R^2 = 0.44) (R^2 range between 0.22 [±0.18] to 0.55 [±0.12]) between $g_{A\text{-}BM13}$ and $g_{A\text{-}STIC}$ with regression parameters ranging between 0.81 (±0.023) and 1.07 (±0.047) for the slope and 0.0019 (±0.0006) to 0.0006 (±0.0006) m s^{-1} for the offset (Table 2). The root mean square deviation (RMSD) varied between 0.007 (TDF) and 0.013 m s^{-1} (TRF). Statistical comparisons between $g_{A\text{-}STIC}$ and $g_{A\text{-}HYB}$ revealed relatively low RMSD and high correlation between them (RMSD = 0.007 m s^{-1} and R^2 = 0.77) as compared to the error statistics between $g_{A\text{-}STIC}$ and $g_{A\text{-}INV}$ (RMSD = 0.011 m s^{-1} and R^2 = 0.50) (Fig. 2b, 2c). The residuals between $g_{A\text{-}STIC}$ and $g_{A\text{-}BM13}$ are plotted as a function of u and u^* in Figure 2d. The aim of this analysis is to show whether there are significant biases introduced by ignoring wind and shear information within STIC. As illustrated in Fig. 2d, there appears to be a weak systematic relationship between the residual g_A difference with either u^* or u (r = -0.26 and -0.17). However, a considerable relationship was found between wind and shear driven g_A (i.e., $g_{A\text{-}BM13}$) versus ϕ, T_R and D_A (r = 0.83, 0.48, and 0.42) (Fig. 2e and 2f), which indicates that these three energy and water constraints can explain 69%, 23%, and 17% variance of $g_{A\text{-}BM13}$.

Canopy-scale evaluation of hourly g_C is presented in Fig. 3a (and Table 2) combining data from the four PFTs. Estimated values range between zero and 0.06 m s^{-1} for $g_{C\text{-}STIC}$ and show reasonable correlation (R^2 = 0.39) (R^2 range between 0.14 [±0.04] to 0.58 [±0.12]) between $g_{C\text{-}STIC}$ and $g_{C\text{-}INV}$ with regression parameters ranging between 0.30 (±0.022) and 0.85 (±0.025) for the slope and 0.0024 (±0.0003) to 0.0097 (±0.0007) m s^{-1} for the offset (Table 2). The root mean square deviation (RMSD) varied between 0.007 (PAS) and 0.012 m s^{-1}

Hydrol. Earth Syst. Sci. Discuss., doi:10.5194/hess-2015-552, 2016
Manuscript under review for journal Hydrol. Earth Syst. Sci.
Published: 27 January 2016

311 (TRF and TDF). Given g_A significantly controls g_C, we also examined whether biases in g_C
312 are introduced by ignoring wind and shear information within STIC. The scatterplots between
313 residual g_C difference ($g_{C\text{-}STIC} - g_{C\text{-}INV}$) versus both u and u^* (Fig. 3b) showed g_C residuals to
314 be evenly distributed across the entire range of u and u^* and no systematic pattern was
315 evident.

316 The reliability of the STIC based g_A and g_C retrievals was further verified by evaluating λE
317 and H estimates (Fig. 4). Both the predicted λE and H are generally in good agreement with
318 the observations, with substantial correlation (r) (R^2 from 0.61 to 0.94), acceptable root mean
319 square deviation (RMSD) of 33 and 37 W m^{-2}, and mean absolute percent deviation (MAPD)
320 of 14% and 32% between the observed and STIC fluxes (Fig. 4). Regression parameters
321 varied between 0.96 (±0.008) to 1.14 (±0.010) for the slope and -16 (±2) to -2 (±2) W m^{-2} for
322 the offset for λE (Table 3), whereas for H, these were 0.60 (±0.025) to 0.89 (±0.035) for the
323 slope and 9 (±1) to 29 (±2) W m^{-2} for the offset (Table 3), respectively. The RMSD in λE
324 varied from 20 to 31 W m^{-2} and 23 to 34 W m^{-2} for H (Table 3).

325 The evaluation of the conductances and surface energy fluxes indicates some efficacy for the
326 STIC derived fluxes and conductance estimates which represent a weighted average of these
327 variables over the source area around EC tower. As a result we feel some justification for
328 exploring the canopy-scale biophysical controls on λE_T and λE_E generated through the STIC
329 framework.

330 **4.2 Canopy coupling, transpiration and evaporation**

331 Given both g_A and g_C are the independent estimates in STIC, the concept of 'decoupling
332 coefficient' (Ω) (Jarvis and McNaughton, 1986) [$\Omega = (s/\gamma + 1)/(s/\gamma + 1 + g_A/g_C)$] was used to
333 understand the degree of biophysical controls on λE_T, which indicates the extent to which the
334 transpiration fluxes are approaching the equilibrium limit. From Fig. 5a an overall weak to

Hydrol. Earth Syst. Sci. Discuss., doi:10.5194/hess-2015-552, 2016
Manuscript under review for journal Hydrol. Earth Syst. Sci.
Published: 27 January 2016

Hydrology and Earth System Sciences
Discussions

moderate relationship (r = -0.31 to -0.42) is apparent between the coupling (i.e., 1-Ω) and λE_T, where λE_T is negatively related to the coupling for all the PFTs, thus indicating the influence of weak to moderate biophysical control on λE_T throughout the year in addition to the radiative controls. The biophysical control was substantially enhanced in TRF (r increased from -0.36 to -0.53 and -0.60) (47 to 67% increase) and TMF (r increased from -0.31 to -0.53 and -0.58) (70 to 85% increase) during the dry seasons (July-September) (Fig. 5a). A profound increase of biophysical control on λE_T during the dry season was also found in TDF (52% increase) and PAS (37% increase) (Fig. 5a). The negative relationship (r = -0.29 to -0.45) between (1-Ω) and λE_E (Fig. 5b) in all four PFTs indicated the role of aerodynamic control on λE_E. The aerodynamic control was also enhanced during the dry seasons as shown by the increased negative correlation (r = -0.50 to -0.69) (Fig. 5b) between (1-Ω) and λE_E.

Illustrative examples of the diurnal variations of λE_E, λE_T, and Ω for two different PFTs with different annual rainfall (2329 mm in rainforest, K34 and 1597 in pasture, FNS) for three consecutive days during both dry and wet seasons are shown in Fig. 5c to 5f. This shows morning rise of Ω and a near-constant afternoon Ω in the wet season (Fig. 5c and 5d), thus indicating no biophysical controls on λE_E and λE_T during this season. On the contrary, during the dry season, the morning rise in Ω is followed by a decrease during noontime (15% to 25% increase in coupling in forest and pasture) (Fig. 5e and 5f) due to dominant biophysical control, which is further accompanied by a transient increase from mid-afternoon till late afternoon and steadily declined thereafter. Interestingly, coupling was relative higher in pasture during the dry seasons the reasons of which is detailed in the following section and discussion.

Hydrol. Earth Syst. Sci. Discuss., doi:10.5194/hess-2015-552, 2016
Manuscript under review for journal Hydrol. Earth Syst. Sci.
Published: 27 January 2016

4.3 g_C and g_A versus transpiration and evaporation

Scatter plots between λE_T and λE_E versus g_C and g_A showed a triangular pattern which became wider with increasing the conductances (Fig. 6). To explain this typical behaviour of λE_T versus g_C and g_A, we further examined the entire mechanism of conductance-λE_T interactions through two dimensional scatters between λE_T and conductances for two consecutive diurnal cycles during wet and dry seasons over rainforest and pasture sites with different annual rainfall (e.g., K34 as wet and FNS as dry site, annual rainfall 2329 mm and 1597 mm) (Fig. 7). Our results confirm the occurrence of diurnal hysteresis between g_C-g_A and λE_T and explain the reason for the shape of the curves obtained in Fig. 6. During the wet season, a distinct environmental control is detectable on g_C and λE_T in the morning hours (Fig. 7a and 7b) in both PFTs where g_C and λE_T increased as a result of increasing R_N, T_R, and D_A. From the late morning to afternoon, a near-constant (forest) or negligible increase (pasture) of λE_T is observed despite substantial reduction of both g_C and g_A (25 to 50% decrease), after which λE_T starts decreasing. This behaviour of λE_T was triggered due to the concurrent changes in R_N (15 to 50% change), D_A (20 to 60% change) and surface temperature (T_R) (5% to 14% change), which indicates the absence of any dominant biophysical regulation on λE_T during the wet season (Fig. 7a and 7b). On the contrary in the dry season, although the morning rise in λE_T is steadily controlled by the integrated influence of environmental variables, but a modest to strong biophysical control is found for both PFTs during the afternoon where λE_T substantially decreased with decreasing conductances (Fig. 7c and 7d). This decrease in λE_T is mainly caused by the reduction in g_C as a result of increasing D_A and T_R (as seen later in Fig. 8a and 8c). In the dry season, the area under the hysteretic relationship between λE_T, g_C and environmental variables was substantially wider in pasture (Fig. 7d) than for the rainforest (Fig. 7c), which is attributed to greater hysteresis area between R_N and D_A in pasture as a result of reduced water supply. The stronger

Hydrol. Earth Syst. Sci. Discuss., doi:10.5194/hess-2015-552, 2016
Manuscript under review for journal Hydrol. Earth Syst. Sci.
Published: 27 January 2016

383 hysteresis effects in pasture during the dry season (Fig. 7d) ultimately led to the stronger
384 relationship between coupling and λE_T (as seen in Fig. 5a).

385 **4.4 Factors affecting variability *of* g_C and g_A**

386 The sensitivity of stomatal conductance to vapor pressure deficit is a key governing factor of
387 transpiration (Ocheltree et al., 2014; Monteith, 1995). We examined if the feedback or feed-
388 forward response hypothesis (Monteith, 1995; Farquhar, 1987) between g_C, D_A, and λE_T is
389 reflected in our canopy-scale g_C retrievals. Combining data of all PFTs, we found an
390 exponential decline of g_C in response to increasing D_A regardless of the variations of net
391 radiation (Fig. 8a). High g_C is consistent with high humidity and low evaporative demand.
392 Five negatively logarithmic scatters fit the data with r values of 0.38 ($0< R_N <150$ W m^{-2}),
393 0.63 ($150< R_N <300$ W m^{-2}), 0.73 ($300< R_N <450$ W m^{-2}), 0.78 ($450< R_N <600$ W m^{-2}), and
394 0.87 ($R_N >600$ W m^{-2}). The sensitivity of g_C to D_A was at the maximum in the high R_N range
395 beyond 600 W m^{-2} and the sensitivity progressively declined with declining magnitude of R_N
396 (0 – 150 W m^{-2}).

397 Scatter plots between g_C and λE_T for different levels of D_A revealed a linear pattern between
398 them for a wide range of D_A ($20> D_A >0$ hPa) (Fig. 8b). Following Monteith (1995), isopleths
399 of R_N are delineated by the solid lines passing through λE_T on the x-axis and through g_C on
400 the y-axis. Isobars of D_A (dotted lines) pass through the origin because λE_T approaches zero
401 as g_C approaches zero. Fig. 8b shows substantial reduction of g_C with increasing D_A without
402 any increase of λE_T, like an inverse hyperbolic pattern to D_A (Monteith 1995; Jones, 1998).
403 For all the PFTs, an active biological (i.e., stomatal) regulation maintained almost constant
404 λE_T when D_A was changed from low to high values (Fig. 8b). At high D_A (above 10 hPa),
405 after an initial increase of λE_T with g_C, g_C approached a maximum limit and remained nearly
406 independent of λE_T (Fig. 8b). Among all the D_A levels, the maximum control of g_C on λE_T

Hydrol. Earth Syst. Sci. Discuss., doi:10.5194/hess-2015-552, 2016
Manuscript under review for journal Hydrol. Earth Syst. Sci.
Published: 27 January 2016

Hydrology and Earth System Sciences
Discussions

variability (62 to 80%) was found at high atmospheric water demand (i.e., 30 hPa>D_A>20 hPa). The scatter plots between g_C and radiometric surface temperature (T_R) (Fig. 8c) for different levels of D_A revealed an exponential decline in g_C with increasing T_R and atmospheric water demand. When retrieved g_A was plotted against the radiometric surface temperature and air temperature difference ($T_R - T_A$), an exponential decline in g_A was found in response to increasing ($T_R - T_A$) (Fig. 8d). High g_A is persistent with low ($T_R - T_A$) irrespective of the variations in R_N (with the exception of very low R_N). Four negatively logarithmic scatters fit g_A versus ($T_R - T_A$) relationship with r values of 0.28 (150< R_N <300 W m^{-2}), 0.55 (3000< R_N <450 W m^{-2}), 0.64 (450< R_N <600 W m^{-2}), and 0.77 (R_N >600 W m^{-2}).

5 Discussion

In this paper, we have estimated the canopy-scale biophysical conductances and quantified their controls on the terrestrial evaporation components in a simplified surface energy balance modeling perspective that treats the canopy as 'big leaf'. The aerodynamic conductance retrieved with STIC showed acceptable correlation and valid estimates of g_A when compared against an empirical model that uses u^* and u to derive g_A (Fig. 1 and 2a) and two other inversion/hybrid-based g_A estimates. The differences between $g_{A\text{-}STIC}$ and $g_{A\text{-}BM13}$ were mainly attributed to the structural differences and empirical nature of the parameterization for the near-surface boundary layer conductance ($(2/ku^{*2})(S_c/P_r)^{0.67}$) in $g_{A\text{-}BM13}$, which results in some discrepancies between $g_{A\text{-}STIC}$ and $g_{A\text{-}BM13}$ particularly in the pasture (Fig. 2a). The turbulent conductance equation (u^{*2}/u) in $g_{A\text{-}BM13}$ is also very sensitive to the uncertainties in the sonic anemometer measurement (Contini et al., 2006; Richiardone et al., 2012). However, the evidence of a weak systematic relationship between the g_A residuals and u (Fig. 2d) and capability of the environmental variables (particularly ϕ, T_R, and D_A) in capturing the variability of $g_{A\text{-}BM13}$ (Fig. 2e and 2f) indicates that $g_{A\text{-}STIC}$ estimates are reliable despite

Hydrol. Earth Syst. Sci. Discuss., doi:10.5194/hess-2015-552, 2016
Manuscript under review for journal Hydrol. Earth Syst. Sci.
Published: 27 January 2016

neglecting u. Excluding u might introduce errors in cases where wind is the only source of variations in g_A and surface fluxes (Mallick et al., 2015). In general, the accuracies in commonly used parametric g_A estimates based on u and surface roughness parameters several meters distant from canopy foliage is limited due to the uncertainties concerning the attenuation of u close to the vegetation surface (Meinzer et al., 1997; Prihodko et al., 2008). The magnitude of u near the foliage can be substantially lower than that measured considerably away at some reference location above or within the canopy (Meinzer et al., 1997). Notwithstanding the inequalities of g_A estimated with different methods, it is challenging to infer the accuracy of the different estimates. However, from the surface flux validation results (Fig. 4) it appears that $g_{A\text{-}STIC}$ is the appropriate aerodynamic conductance satisfying the PM equation. Discrepancies between $g_{C\text{-}STIC}$ and $g_{C\text{-}INV}$ originated from the differences in g_A estimates between the two methods.

Despite the good agreement between the measured and predicted λE and H (Fig. 4, Table 3), the larger error in H was associated with the higher sensitivity of H to the errors in T_R (due to poor emissivity correction) (Mallick et al., 2015). Since the difference between T_R and T_A is considered to be the primary driving force of H (van der Tol et al., 2009), the modelled errors in H are expected to arise due to the uncertainties associated with T_R.

The correlation analysis between 1-Ω and λE_T revealed the extent of biophysical and radiative controls on λE_T (Fig. 5). The degree of biophysical control is a function of the ratio of g_C to g_A. Minor biophysical control on λE_T was apparent for forest and pasture during the wet seasons (Fig. 5c and 5d) as a result of a high g_C/g_A ratio along with increasing λE_T. Such conditions stimulate local humidification of air surrounding the canopy and uncoupling of the in-canopy vapor pressure deficit (D_0) from that in the air above (i.e., $D_0<D_A$) (Meinzer et al., 1997; Motzer et al., 2005) (Fig. 9a), which implies that λE_T becomes largely independent of

Hydrol. Earth Syst. Sci. Discuss., doi:10.5194/hess-2015-552, 2016
Manuscript under review for journal Hydrol. Earth Syst. Sci.
Published: 27 January 2016

Hydrology and Earth System Sciences
Discussions

456 g_C. On the contrary, an enhanced biophysical control on λE_T was apparent during the dry
457 season and drought year 2005 during the period of reduced water supply particularly over
458 PAS (Fig. 5e, 5f, and 7). Such condition leads to a relatively dry canopy surface, and
459 substantially high g_A compared to g_C, thus resulting in low g_C/g_A ratios regardless of their
460 absolute values (Meinzer et al., 1993; McNaughton and Jarvis, 1991). Here, fractional
461 changes in g_C results in an equivalent fractional change in λE_T. This impedes transpiration
462 from promoting local equilibrium of D_0 and minimizing (or maximizing) the gradient
463 between D_0 and atmospheric vapor pressure deficit (D_A) (i.e., $D_0 \cong D_A$ or $D_0 > D_A$) (eq. A3) (Fig
464 9a), thereby resulting in strong coupling between D_0 and D_A (Meinzer et al., 1993; Jarvis and
465 McNaughton, 1986). Besides, a supplemental biophysical control on λE_T might have been
466 imposed as a consequence of a direct negative feedback of D_A and D_0 on g_C (McNaughton
467 and Jarvis, 1991; Jarvis, 1986). Increase in D_A (or D_0) beyond a certain limit decreases g_C
468 (Fig. 7 and 8), resulting in a low and narrow increase of λE_T, despite steady increase in g_A and
469 R_N. The combination of negative feedback response between D_A and g_C with the overall
470 radiative-aerodynamic coupling significantly dampens the variation of transpiration in PAS
471 and TDF in the dry season, thus featuring increased biophysical control in these PFTs. These
472 results are in agreement with von Randow et al. (2012), who found enhanced biophysical
473 control on λE_T for the pasture during the dry season. For the wet season, evidence of minor
474 biophysical control indicates the dominance of R_N driven equilibrium evaporation in these
475 PFTs (Hasler and Avissar, 2007; da Rocha et al., 2009; Costa et al., 2010). In the TRF and
476 TMF, 94% and 99% of the retrieved g_C/g_A ratio fall above 0.5, and, only 1% and 6% of the
477 retrieved g_C/g_A ratio fall below the 0.5 range (Fig. 9b). In contrast, 90% and 73% of the g_C/g_A
478 ratio values range above 0.5, and 10% to 27% of the g_C/g_A ratio below 0.5 for TDF and PAS,
479 respectively (Fig. 9b). This shows that, although radiation control is prevailing in all the sites,
480 biophysical control is relatively stronger in TDF and PAS as compared to the other sites. For

Hydrol. Earth Syst. Sci. Discuss., doi:10.5194/hess-2015-552, 2016
Manuscript under review for journal Hydrol. Earth Syst. Sci.
Published: 27 January 2016

large g_C/g_A ratios, the conditions within the planetary boundary layer (PBL) become decoupled from the synoptic scale (McNaughton and Jarvis, 1991) and the net radiative energy becomes the important regulator of transpiration. For small g_C/g_A ratios (e.g., in dry season), the conditions within the PBL are strongly coupled to the atmosphere above by rapid entrainment of air from the capping inversion and by some ancillary effects of sensible heat flux on the entrainment (McNaughton and Jarvis, 1991). These findings substantiates the earlier theory of McNaughton and Jarvis (1991), who postulated that large g_C/g_A ratios result in minor biophysical control on canopy transpiration due to the negative feedback on the canopy from the PBL. The negative relationship between 1-Ω and λE_E (Fig. 5b) over all the PFTs is due to the feedback of g_A on g_C. However, over all the PFTs, a combined control of g_A and environmental variables on λE_E again highlighted the impact of realistically estimated g_A on λE_E (Holwerda et al., 2012).

It is important to mention that forests are generally expected to be better coupled to the atmosphere, which is related to generally higher g_A/g_C ratios compared to the pastures. This implies that forests exhibit stronger biophysical control on λE_T. However, due to the broad leaves of the rain forests (larger leaf area index) and higher surface wetness (due to higher rainfall amounts) the wet surface area is much larger in the forest than in the pastures. This results in much higher g_C values for forests than for pastures during the wet season, and $g_C/g_A \rightarrow 1$. Consequently, no significant difference in coupling was found between them during the wet season (Fig. 5c and 5d). Despite the absolute differences in g_A and g_C between forest and pasture, the high surface wetness is largely offsetting the expected Ω difference between them. Although the surface wetness is substantially lower during the dry season, the high water availability in the forests due to the deeper root systems help maintaining a relatively high g_C compared to the pastures. Hence, despite g_A (forest) > g_A (pasture) during the dry season, substantially lower g_C values for the pasture result in lower g_C/g_A ratio for the pasture

Hydrol. Earth Syst. Sci. Discuss., doi:10.5194/hess-2015-552, 2016
Manuscript under review for journal Hydrol. Earth Syst. Sci.
Published: 27 January 2016

compared to the forest, thus causing more biophysical control on λE_T during the dry season. The relatively better relationship between coupling versus λE_T in PAS and TDF during the dry season was also attributed to high surface air temperature difference ($T_R - T_A$) in these PFTs that resulted in low g_C/g_A ratios (Fig. 9c).

The stomatal feedback-response hypothesis (Monteith, 1995) also became apparent at the canopy-scale (Fig. 8a, 8b), which states that a decrease in g_C with increasing D_A is caused by a direct increase in λE_T (Monteith, 1995; Matzner & Comstock, 2001; Streck, 2003) and g_C responds to the changes in the air humidity by sensing λE_T, rather than D_A. This feedback mechanism is found because of the influence of D_A on both g_C and λE_T, which in turn changes D_A by influencing the air humidity (Monteith, 1995). The change in g_C is dominated by an increase in the net available energy, which is partially offset by an increase in λE_T. After the net energy input in the canopy exceeds a certain threshold, g_C starts decreasing even if λE_T increases. High λE_T increases the water potential gradient between guard cells and other epidermal cells or reduces the bulk leaf water potential, thus causing stomatal closure (Monteith, 1995; Jones, 1998; Streck, 2003). The control of soil water on transpiration also became evident from the scatters between g_C versus λE_T and T_R for different D_A levels (Fig. 8b, 8c) (also Fig. 7). Denmead and Shaw (1962) hypothesized that reduced g_C and stomatal closure occurs at moderate to higher levels of soil moisture (high λE_T) when the atmospheric demand of water vapor increases (high D_A). The water content in the immediate vicinity of the plant root depletes rapidly at high D_A, which decreases the hydraulic conductivity of soil, and the soil is unable to efficiently supply water under these conditions. For a given evaporative demand and available energy, transpiration is determined by the g_C/g_A ratio, which is further modulated by the soil water availability. These combined effects tend to

Hydrol. Earth Syst. Sci. Discuss., doi:10.5194/hess-2015-552, 2016
Manuscript under review for journal Hydrol. Earth Syst. Sci.
Published: 27 January 2016

529 strengthen the biological control on transpiration (Leuzinger and Kirner, 2010; Migletta et al.,
530 2011).

531 Fig. 8d is in accordance with existing theory that under conditions of extremely high
532 atmospheric turbulence (i.e., high g_A), a close coupling exists between the surface and the
533 atmosphere, which causes T_R and T_A to converge (i.e., $T_R - T_A \rightarrow 0$). When g_A is low, the
534 difference between T_R and T_A increases due to poor vertical mixing of the air.

535 ## 6 Conclusions

536 Stomata regulate the coupling between terrestrial carbon and water cycles, which implies that
537 their behaviour under global environmental change is decisive to predict vegetation
538 functioning (Medlyn et al., 2011). The combination of progressing rainfall reduction (Hilker
539 et al., 2014) and land cover change (Davidson et al., 2012) in the Amazon Basin is expected
540 to increase the canopy-atmosphere coupling of pasture or forest under drier conditions by
541 altering the ratio of the biological and aerodynamic conductances. Increase of biophysical
542 control will most likely be an indicator of shifting the transpiration pool from an energy-
543 limited to a water-limited regime (due to the impact of T_R, T_A, and D_A on the g_C/g_A ratio) with
544 further consequences for the surface water balance and rainfall recycling. At the same time,
545 transition from forest to pasture or agriculture will substantially reduce the contribution of
546 interception evaporation in the Amazon, hence, it will affect the regional water cycle. This
547 might change the moisture regime of the Amazonian Basin and affect the moisture transport
548 to other regions. STIC provides a new quantitative and internally consistent method for
549 interpreting the biophysical conductances across a broad spectrum of PFTs in response to a
550 range of climatic and ecohydrological conditions (excluding rising atmospheric CO_2). It
551 could also provide the basis to improve existing land surface parameterisations for simulating
552 vegetation water use at large spatial scales. However, it should also be noted that although the
553 case study described here provides general insights into the biophysical controls of λE and

Hydrol. Earth Syst. Sci. Discuss., doi:10.5194/hess-2015-552, 2016
Manuscript under review for journal Hydrol. Earth Syst. Sci.
Published: 27 January 2016

associated feedback between g_C, D_A, T_R and λE_T in the framework of the PM equation, there is a tendency of g_C overestimation due to the entangling evaporation information in the current single-source framework of STIC1.2. For accurate characterisation of canopy conductance, explicit partitioning of λE into transpiration and evaporation (both soil and interception) is one of the further scopes for improving STIC1.2 and this assumption needs to be tested further.

Acknowledgements

This study was funded by the Luxembourg Institute of Science and Technology (LIST). We sincere thank Dr. Andrew Jarvis (Lancaster University, UK) and Dr. Georg Wohlfahrt (University of Innsbruck, Austria) for very helpful discussions and edits in the manuscript. We are grateful to all Brazilian and international collaborators and all the funding agencies that have contributed to the Large-scale Biosphere Atmosphere Experiment in Amazônia (LBA). The authors are indebted to Pavel Kabat, Antônio Ocimar Manzi, David R. Fitzjarrald, Julio Tota, Humberto Ribeiro da Rocha, Michael Goulden, Maarten J. Waterloo and Luiz Martinelli for planning, coordinating, conducting, and evaluating the eddy covariance, meteorological and leaf gas exchange measurements at the LBA sites. We are particularly grateful to all field technicians whose hard work were the key ingredients to establish the quality of the datasets used in this paper. The authors declare no conflict of interest.

Appendix:

Derivation of *M*

The retrieval of M is already described in Mallick et al. (2015) (as adopted from Venturini et al., 2008). We hypothesize that the moisture availability at the surface and at the evaporating front are uniform and, therefore, M is derived from the surface-atmosphere information.

Hydrol. Earth Syst. Sci. Discuss., doi:10.5194/hess-2015-552, 2016
Manuscript under review for journal Hydrol. Earth Syst. Sci.
Published: 27 January 2016

Hydrology and Earth System Sciences
Discussions

Following Venturini et al. (2008), M can be expressed as the ratio of the vapor pressure difference to the vapor press deficit between surface to atmosphere as follows.

$$M = \frac{(e_0 - e_A)}{(e_0^* - e_A)} = \frac{s_1(T_{SD} - T_D)}{s_2(T_0 - T_D)} \quad \text{(A1)}$$

Where T_{SD} is the dewpoint temperature of the evaporating front and T_D is the air dewpoint temperature, s_1 and s_2 are the psychrometric slopes of the saturation vapor pressure and temperature between $(T_{SD} - T_D)$ versus $(e_0 - e_A)$ and $(T_0 - T_D)$ versus $(e_0^* - e_A)$ relationship (Venturini et al., 2008). Since T_0 is not available and T_R and e_A are available, we compute s_2 as $s_2 = (e_s^* - e_A)/(T_R - T_D)$ with the assumption that errors due to any inequality between T_0 versus T_R and e_0^* versus e_s^* will be cancelled in this ratio. This appears to be a valid assumption due to the close relationship between T_0 and T_R (Huband and Monteith, 1986). In eq. A1, T_{SD} computation is challenging because both e_0 and s_1 are unknown. By decomposing the aerodynamic equation of λE, T_{SD} can be expressed as follows.

$$\lambda E = \frac{\rho c_P}{\gamma} g_A (e_0 - e_A) = \frac{\rho c_P}{\gamma} g_A s_1 (T_{SD} - T_D)$$

$$T_{SD} = T_D + \frac{\gamma \lambda E}{\rho c_P g_A s_1} \quad \text{(A2)}$$

In the earlier STIC versions, s_1 was approximated at T_D, T_{SD} was estimated from s_1, T_D, T_R, and related saturation vapor pressures (Mallick et al., 2014; 2015), and M was estimated from eq. A1. However, since T_{SD} depends on λE and g_A, an iterative procedure is now applied to estimate T_{SD} and M as described below, which is another modification of the STIC1.0 and STIC1.1.

STIC1.2

In STIC1.0 and 1.1 (Mallick et al., 2014; 2015), no distinction was made between the surface and source/sink height vapor pressures. Therefore, e_0^* was approximated as the saturation vapor pressure at T_R and e_0 was empirically estimated from M based on the assumption that the vapor pressure at the source/sink height ranges between extreme wet–dry surface

Hydrol. Earth Syst. Sci. Discuss., doi:10.5194/hess-2015-552, 2016
Manuscript under review for journal Hydrol. Earth Syst. Sci.
Published: 27 January 2016

Hydrology and Earth System Sciences
Discussions

599 conditions. However, the level of e_0 and e_0^* should be consistent with the level of the
600 aerodynamic temperature (T_0) from which the sensible heat flux is transferred (Lhomme and
601 Montes, 2014). The predictive use of the PM model could be hindered due to neglecting the
602 feedbacks between the surface layer evaporative fluxes and source/sink height mixing and
603 coupling (McNaughton and Jarvis, 1984), and their impact on the canopy scale conductances.
604 Therefore, in STIC1.2, we have used physical expressions for estimating e_0 and e_0^* followed
605 by estimating T_{SD} and M as described below.

606 Following Shuttleworth and Wallace (1985) (SW85, hereafter), the vapor pressure deficit
607 (D_0) (=e_0^* - e_0) at the source/sink height is expressed as follows.

$$D_0 = D_A + \left[\frac{\{s\phi - (s + \gamma)\lambda E\}}{\rho c_P g_A}\right] \quad \text{(A3)}$$

608 An estimate of e_0^* is obtained by inverting the aerodynamic transfer equation of λE.

$$e_0^* = e_A + \left[\frac{\gamma \lambda E (g_A + g_C)}{\rho c_P g_A g_C}\right] \quad \text{(A4)}$$

609 A physical equation of α is derived by expressing the evaporative fraction (Λ) as function of
610 the aerodynamic equations of H $[\rho c_P g_A (T_0 - T_A)]$ and λE $[\frac{\rho c_P}{\gamma}\frac{g_A g_C}{g_A + g_C}(e_0^* - e_A)]$ as follows.

$$\Lambda = \frac{\lambda E}{H + \lambda E} \quad \text{(A5)}$$

$$= \frac{\frac{\rho c_P}{\gamma}\frac{g_A g_C}{g_A + g_C}(e_0^* - e_A)}{\rho c_P g_A (T_0 - T_A) + \frac{\rho c_P}{\gamma}\frac{g_A g_C}{g_A + g_C}(e_0^* - e_A)} \quad \text{(A6)}$$

$$= \frac{g_C (e_0^* - e_A)}{[\gamma (T_0 - T_A)(g_A + g_C) + g_C (e_0^* - e_A)]} \quad \text{(A7)}$$

611 Combining eq. A7 and eq. 5, we can derive a physical expression of α as follows.

Hydrol. Earth Syst. Sci. Discuss., doi:10.5194/hess-2015-552, 2016
Manuscript under review for journal Hydrol. Earth Syst. Sci.
Published: 27 January 2016

Hydrology and Earth System Sciences
Discussions

$$\alpha = \frac{g_C(e_0^* - e_A)\left[2s + 2\gamma + \gamma\frac{g_A}{g_C}(1+M)\right]}{2s[\gamma(T_0 - T_A)(g_A + g_C) + g_C(e_0^* - e_A)]} \quad \text{(A8)}$$

In STIC1.2, an initial value of α is assigned as 1.26 and initial estimates of e_0^* and e_0 are obtained from T_R and M as $e_0^* = 6.13753e^{\frac{17.27T_R}{(T_R+237.3)}}$ and $e_0 = e_A + M(e_0^* - e_A)$. Initial T_{SD} and M were estimated as described in the earlier section. With the initial estimates of these variables; first estimate of the conductances, T_0, Λ, and λE are derived. The process is then iterated by updating D_0 (using eq. A3), e_0^* (using eq. A4), e_0 ($e_0 = e_0^* - D_0$), T_{SD} (using eq. A2 with s_1 estimated at T_D), M [$M = s_1(T_{SD} - T_D)/s_2(T_R - T_D)$], and α (using eq. A8), with the first estimates of g_C, g_A, and λE, and recomputing g_A, g_C, T_0, Λ, and λE in the subsequent iterations with the previous estimates of e_0^*, e_0, T_{SD}, M, and α until convergence of these variables is achieved. Stable values of e_0^*, e_0, T_{SD}, M, and α are obtained with ~25 iterations. Illustrative examples of the convergence of e_0^*, e_0, T_{SD}, M, and α are shown in Fig. A2.

To summarize, the computational steps of the conductances and evaporative fluxes in STIC are:

Step 1: Analytical solution of the conductances, T_0 and Λ by solving the state equations (eq. 2 to 5). Step 2: Initial estimates of the conductances (g_C and g_A), T_0, Λ, and λE. Step 3: Simultaneous iteration of e_0^*, e_0, T_{SD}, M, and α; and final estimation of the conductances (g_C and g_A), T_0, Λ, λE and H. Step 4: Partitioning λE into λE_T and λE_E.

References:

Andreae, M.O., Artaxo, P., Brandao, C., et al.: Biogeochemical cycling of carbon, water, energy, trace gases, and aerosols in Amazonia: The LBA-EUSTACH experiments, J. Geophys. Res., 107, D20, 8066, doi:10.1029/2001JD000524, 2002.

632 Baker, I.T., Harper, A.B., da Rocha, H.R., Denning, A.S., et al.: Surface ecophysiological
633 behavior across vegetation and moisture gradients in tropical South America, Agric. For.
634 Meteorol., 182– 183, 177– 188, 2013.

635 Baldocchi, D.D., Wilson, K., and Gu, L.: How the environment, canopy structure and canopy
636 physiological functioning influence carbon, water and energy fluxes of a temperate
637 broad-leaved deciduous forest-An assessment with the biophysical model CANOAK,
638 Tree Phys., 22(15–16), 1065, 2002.

639 Baldocchi, D.D., and Ma, S.: How will land use affect air temperature in the surface
640 boundary layer? Lessons learned from a comparative study on the energy balance of an
641 oak savanna and annual grassland in California, USA, Tellus B, 65, 19994,
642 http://dx.doi.org/10.3402/tellusb.v65i0.19994, 2013.

643 Ball, J.T., Woodrow, I.E., and Berry, J.A.: A model predicting stomatal conductance and its
644 contribution to the control of photosynthesis under different environmental conditions.
645 *In: Progress in Photosynthesis Research*, ed. J Biggins. M Nijhoff, Dordrecht, *4*, 5.221-
646 5.224, Martinus-Nijhoff Publishers, Dordrecht, The Netherlands, 1987.

647 Blyth, E., Gash, J., Lloyd, A., Pryor, M., Weedon, G.P., and Shuttleworth, W.J.: Evaluating
648 the JULES Land Surface Model Energy Fluxes Using FLUXNET Data, J.
649 Hydrometeorol., 11, 509–519, doi: http://dx.doi.org/10.1175/2009JHM1183.1, 2010.

650 Bonan, G.B., Williams, M., Fisher, R.A., and Oleson, K.W.: Modeling stomatal conductance
651 in the earth system: linking leaf water-use efficiency and water transport along the soil–
652 plant–atmosphere continuum, Geosci. Model Development, 7, 2193–2222,
653 doi:10.5194/gmd-7-2193-2014, 2014.

654 Bosveld, F.C., and Bouten, W.: Evaluating a model of evaporation and transpiration with
655 observations in a partially wet Douglas-fir forest, Boundary Layer Meteorol., 108, 365 –
656 396, 2003.

657 Boulet, G., Mougenot, B., Lhomme, J.-P., Fanise, P., Lili-Chabaane, Z., Olioso, A., Bahir,
658 M., Rivalland, V., Jarlan, L., Merlin, O., Coudert, B., Er-Raki, S., and Lagouarde, J.-P.:
659 The SPARSE model for the prediction of water stress and evapotranspiration
660 components from thermal infra-red data and its evaluation over irrigated and rainfed
661 wheat, Hydrol. Earth Syst. Sci., 19, 4653-4672, doi:10.5194/hess-19-4653-2015, 2015.

662 Christoffersen, B.O., Restrepo-Coupe, N., Arain, M.A., and Baker, I.T., et al.: Mechanisms of
663 water supply and vegetation demand govern the seasonality and magnitude of
664 evapotranspiration in Amazonia and Cerrado, Agric. For. Meteorol., 191, 33 – 50, 2014.

665 Colaizzi, P.D., Kustas, W.P., and Anderson, M.C., et al.: Two-source energy balance model
666 estimates of evapotranspiration using component and composite surface temperatures,
667 Adv. Water Resour., 50, 134-151, 2012.

668 Contini, D., Donateo, A., and Belosi, F.: Accuracy of Measurements of Turbulent Phenomena
669 in the Surface Layer with an Ultrasonic Anemometer, J. Atm. Oceanic Tech., 23, 785–
670 801, doi: http://dx.doi.org/10.1175/JTECH1881.1, 2006.

671 Costa, M.H., Biajoli, M.C., Sanches, L., Malhado, A.C.M. et al. : Atmospheric versus
672 vegetation controls of Amazonian tropical rain forest evapotranspiration: Are the wet
673 and seasonally dry rain forests any different?, J. Geophys. Res. – Biogeosci., 115,
674 G04021, doi: 10.1029/2009JG001179, 2010.

675 Cox, P.M., Betts, R.A., Jones, C.D., Spall, S.A., and Totterdell, I.J.: Acceleration of global
676 warming due to carbon-cycle feedbacks in a coupled climate model, Nature, 408, 184 –
677 187, 2000.

678 da Rocha, H.R., Manzi, A.O., Cabral, O.M. et al.: Patterns of water and heat flux across a
679 biome gradient from tropical forest to savanna in Brazil. J. Geophys. Res. – Biogeosci.,
680 114, G00B12, doi:10.1029/2007JG000640, 2009.

681 da Rocha, H.R., Goulden, M., Miller, S., Menton, M., Pinto, L., Freitas, H., and Figueira,
682 A.S.: Seasonality of water and heat fluxes over a tropical forest in eastern Amazonia,
683 Ecol. Appl., 14(4), 22– 32, 2004.

684 Davidson, E.A., de Araújo, A.C., Artaxo, P. et al.: The Amazon basin in transition, *Nature*,
685 481(7381), 321–328, 2012.

686 Denmead, O.T., and Shaw, R.H.: Availability of soil water to plants as affected by soil
687 moisture content and meteorological conditions, Agron. J., 54, 385–390, 1962.

688 Dolman, A.J., Miralles, D.G., and de Jeu, R.A.M.: Fifty years since Monteith's 1965 seminal
689 paper: the emergence of global ecohydrology, Ecohydrol., 7, 897–902, doi:
690 10.1002/eco.1505, 2014.

691 Drewry, D.T., Kumar, P., Long, S., Bernacchi, C., Liang, X.Z., and Sivapalan, M.:
692 Ecohydrological responses of dense canopies to environmental variability: 1. Interplay
693 between vertical structure and photosynthetic pathway, J. Geophys. Res. – Biogeosci.,
694 115, G04022, doi:10.1029/2010JG001340, 2010.

695 Gatti, L.V., Gloor, M., Miller, J.B., et al.: Drought sensitivity of Amazonian carbon balance
696 revealed by atmospheric measurements, Nature, 506, 76–80, doi:
697 10.1038/nature12957, 2014.

698 Gloor, M., Brienen, R.J.W., Galbraith, D., et al.: Intensification of the Amazon hydrological
699 cycle over the last two decades, Geophys. Res. Let., 40, 1729–1733, 2013.

700 de Goncalves, L.G.G., Borak, J.S., Costa, M.H., Saleska, S.R., et al.: Overview of the Large-
701 Scale Biosphere–Atmosphere Experiment in Amazonia Data Model Intercomparison
702 Project (LBA-DMIP), Agric. For. Meteorol., 182– 183, 111– 127, 2013.

703 Harper, A., Baker, I.T., Denning, A.S., Randall, D.A., Dazlich, D., and Branson, M.: Impact
704 of Evapotranspiration on Dry Season Climate in the Amazon Forest, J. Climate, 27,
705 574–591, doi: http://dx.doi.org/10.1175/JCLI-D-13-00074.1, 2014.

706 Hasler, N., and Avissar, R.: What controls evapotranspiration in the Amazon Basin, J.
707 Hydrometeorol., 8, 380–395, doi: http://dx.doi.org/10.1175/JHM587.1, 2007.

708 Hilker, T., Lyapustin, A.I., Tucker, C.J., et al.: Vegetation dynamics and rainfall sensitivity of
709 the Amazon, Proc. National Academy of Sci., 111 (45), 16041 – 16046, doi:
710 10.1073/pnas.1404870111, 2014.

711 Holwerda, F., Bruijnzeela, L.A., Scatenac, F.N., Vugtsa, H.F., and Meestersa, A.G.C.A.: Wet
712 canopy evaporation from a Puerto Rican lower montane rain forest: the importance of
713 realistically estimated aerodynamic conductance, J. Hydrol., 414-415, 1-15, 2012.

714 Huband, N.D.S., and Monteith, J.L.: Radiative surface temperature and energy balance of a
715 wheat canopy I: Comparison of radiative and aerodynamic canopy temperature,
716 Boundary-Layer Meteorol., *36*, 1-17, 1986.

717 Huntingford, C., Fisher, R.A., Mercado, L., et al.: Towards quantifying uncertainty in
718 predictions of Amazon 'dieback', Phil. Trans. Royal Soc. London. Ser. B, Biol. Sci.,
719 363, 1857–1864, 2008.

720 Jarvis, P.G.: Transpiration and assimilation of trees and agricultural crops: the 'omega'
721 factor. In *Attributes of Trees and Crop Plants*, Edited by Cannell MGR and Jackson JE,
722 Institute of terrestrial Ecology, Edinburg, UK, 460 – 480, 1986.

723 Jarvis, P.G., and McNaughton, K.G.: Stomatal control of transpiration: scaling up from leaf
724 to region, Adv. Ecol. Res., 15, 1 – 49, 1986.

725 Jones, H.G.: Stomatal control of photosynthesis and transpiration, J. Exp. Bot., 49, 387 – 398,
726 1998.

727 Lawrence, D., and Vandecar, K.: Effects of tropical deforestation on climate and agriculture,
728 Nature Clim. Change, 5, 27–36, doi: 10.1038/nclimate2430, 2015.

729 Leuning, R.: A critical appraisal of a combined stomatal – photosynthesis model for c3
730 plants, Pl. Cell and Environ., 18, 339 – 355, 1995.

731 Leuzinger, S., and Kirner, C.: Rainfall distribution is the main driver of runoff under future
732 CO2-concentration in a temperate deciduous forest, Global Change Biol., 16, 246 – 254,
733 2010.

734 Lhomme, J.P., and Montes, C.: Generalized combination equations for canopy evaporation
735 under dry and wet conditions, Hydrol. Earth Sys. Sci., 18, 1137–1149, 2014.

736 Loescher, H.W., Gholz, H.L., Jacobs, J.M., and Oberbauer, S.F.: Energy dynamics and
737 modeled evapotranspiration from a wet tropical forest in Costa Rica, J. Hydrol., 315, 274
738 – 294, 2005.

739 Malhi, Y., Pegoraro, E., Nobre, A.D., Pereira, M.G.P., Grace, J., Culf, A.D., and Clement, R.:
740 The energy and water dynamics of a central Amazonian rain forest, J. Geophys. Res.,
741 107, D20, 10.1029/2001JD000623, 2002.

742 Malhi, Y.: The productivity, metabolism and carbon cycle of tropical forest vegetation, J.
743 Ecol., 100, 65–75, 2012.

744 Mallick, K., Boegh, E., Trebs, I., et al.: Reintroducing radiometric surface temperature into
745 the Penman-Monteith formulation, Water Resour. Res., 51,
746 doi:10.1002/2014WR016106, 2015.

747 Mallick, K., Jarvis, A.J., Boegh, E., et al.: A surface temperature initiated closure (STIC) for
748 surface energy balance fluxes, Remote Sens. Environ., 141, 243 – 261, 2014.

749 Miglietta, F., Peressotti, A., Viola, R., Körner, C., and Amthor, J.S.: Stomatal numbers, leaf
750 and canopy conductance, and the control of transpiration, Proc. National Acad. Sci., 108
751 (28), E275-E275, 2011.

752 Matheny, A.M., Bohrer, G., Stoy, P., Baker, I.T., et al.: Characterizing the diurnal patterns of
753 errors in the prediction of evapotranspiration by several land-surface models: An NACP
754 analysis, J. Geophys. Res.- Biogeosci., 119, doi:10.1002/2014JG002623, 2014.

755 Matzner, S., and Comstock, J.: The temperature dependence of shoot hydraulic resistance:
756 implications for stomatal behaviour and hydraulic limitation, Pl. Cell and Environ., 24
757 (11), 1299 – 1307, 2001.

758 McNaughton, K.G., and Jarvis, P.G.: Using the Penman-Monteith equation predictively,
759 Agric. Water Management, 8 (1-3), 263-278, 1984.

760 McNaughton, K.G., and Jarvis, P.G.: Effects of spatial scale on stomatal control of
761 transpiration, Agric. For. Meteorol., 54, 279 – 301, 1991.

762 Medlyn, B.E., Duursma, R.A., Eamus, D., et al.: Reconciling the optimal and empirical
763 approaches to modelling stomatal conductance, Global Change Biol., doi:
764 10.1111/j.1365-2486.2010.02375.x, 2011.

765 Meinzer, F.C., Andrade, J.L., Goldstein, G., Holbrook, N.M., Cavelier, J., and Jackson, P.:
766 Control of transpiration from upper canopy of a tropical forest: the role of stomatal,
767 boundary layer and hydraulic architecture components, Pl. Cell and Environ., 20, 1242 –
768 1252, 1997.

769 Meinzer, F.C., Goldstein, G., Holbrook, N.M., Jackson, P., Cavelier, J.: Stomatal and
770 environmental control of transpiration in a lowland tropical forest site, Pl. Cell and
771 Environ., 16, 429 – 436, 1993.

772 Mercado, L.M., Lloyd, J., Dolman, A.J., Sitch, S., and Pati, S.: Modelling basin-wide
773 variations in Amazon forest productivity – Part 1: Model calibration, evaluation and
774 upscaling functions for canopy photosynthesis, Biogeosci., 6, 1247-1272, doi:
775 10.5194/bg-6-1247-2009, 2009.

776 Monteith, J.L.: Evaporation and environment. In G.E. Fogg (ed.) *Symposium of the Society*
777 *for Experimental Biology, The State and Movement of Water in Living Organisms, 19,*
778 pp. 205-234. Academic Press, Inc., NY, 1965.

779 Monteith, J.L.: Evaporation and surface temperature, Quart. J. Royal Met. Soc., 107, 1–27,
780 1981.

781 Monteith, J.L.: Accommodation between transpiring vegetation and the convective boundary
782 layer, J. Hydrol., 166, 251 – 263, 1995.

783 Monteith, J.L., and Unsworth, M.H.: *Principles of Environmental Physics*. Elsevier,
784 Amsterdam, 2008.

785 Moran, M.S., Clarke, T.R., Inoue, Y., Vidal, A.: Estimating crop water deficit between
786 surface-air temperature and spectral vegetation index, Remote Sens. Environ., 46, 246-
787 263, 1994.

788 Motzer, T., Munz, N., Kuppers, M., Schmitt, D., and Anhuf, D.: Stomatal conductance,
789 transpiration and sap flow of tropical montane rain forest trees in the southern
790 Ecuadorian Andes, Tree Physiol., 25, 1283 – 1293, 2005.

791 Penman, H.L.: Natural evaporation from open water, bare soil, and grass, Proc. Royal Soc.
792 London, Ser. A, 193, 120–146, 1948.

793 Priante Filho, N., Vourlitis, G.L., Hayashi, M.M.S., de Souza Nogueira, J., et al.: Comparison
794 of the mass and energy exchange of a pasture and a mature transitional tropical forest of

795 the southern Amazon Basin during a seasonal transition, Global Change Biol., 10, 863–
796 876, doi: 10.1111/j.1529-8817.2003.00775.x, 2004.

797 Priestley, C.H.B., and Taylor, R.J.: On the assessment of surface heat flux and evaporation
798 using large scale parameters, Monthly Weather Rev., 100, 81–92, 1972.

799 Prihodko, L., Denning, A.S., Hanan, N.P., Baker, I.T., and Davis, K.: Sensitivity, uncertainty
800 and time dependence of parameters in a complex land surface model, Agric. For.
801 Meteorol., 148 (2), 268–287, 2008.

802 Raupach, M.R.: Vegetation-atmosphere interaction and surface conductance at leaf, canopy
803 and regional scales, Agric. For. Meteorol., 73, 151-179, 1995.

804 Raupach, M.R., and Finnigan, J.J.: Scale issues in boundary-layer meteorology: surface
805 energy balance in heterogeneous terrain, Hydrol. Proc., 9, 589 – 612, 1995.

806 Richiardone, R., Manfrin, M., Ferrarese, S., Francone, C., Fernicola, V., Gavioso, R.M., and
807 Mortarini, L.: Influence of the Sonic Anemometer Temperature Calibration on Turbulent
808 Heat-Flux Measurements, Boundary Layer Meteorol., 142 (3), 425-442, 2012.

809 Roy, S.B., and Avissar, R.: Impact of land use/land cover change on regional
810 hydrometeorology in Amazonia, J. Geophys. Res., 107, D20, doi:
811 10.1029/2000JD000266, 2002.

812 Natalia Restrepo-Coupea, N., da Rocha, H.R., Hutyra, L.R., da Araujo, A.C., et al.: What
813 drives the seasonality of photosynthesis across the Amazon basin? A cross-site analysis
814 of eddy flux tower measurements from the Brasil flux network, Agric. For. Meteorol.,
815 182– 183, 128– 144, 2013.

816 Ocheltree, T.W., Nippert, J.B., and Prasad, P.V.V.: Stomatal responses to changes in vapor
817 pressure deficit reflect tissue-specific differences in hydraulic conductance, Pl. Cell
818 Environ., 37, 132–139, 2014.

819 Saleska, S.R., da Rocha, H.R., Huete, A.R., Nobre, A.D., Artaxo, P., and Shimabukuro, Y.E.:
820 LBA-ECO CD-32 Flux Tower Network Data Compilation, Brazilian Amazon: 1999-
821 2006. Data set. Available on-line [http://daac.ornl.gov] from Oak Ridge National
822 Laboratory Distributed Active Archive Center, Oak Ridge, Tennessee, USA,
823 http://dx.doi.org/10.3334/ORNLDAAC/1174, 2013.

824 Shuttleworth, W.J.: Micrometeorology of temperate and tropical forest, Phil. Trans. Royal
825 Soc. London. Ser. B, Biol. Sci., 324, 299-334, 1989.

826 Shuttleworth, W.J.: Putting the "vap" into evaporation. Hydrol. Earth Sys. Sci., 11, 210-244,
827 doi: 10.5194/hess-11-210-2007, 2007.

828 Shuttleworth, W.J., and Wallace, J.S.: Evaporation from sparse crops – an energy
829 combination theory, Quart. J. Royal Met. Soc., 111, 839 – 855, 1985.

830 Streck, N.A.: Stomatal response to water vapor pressure deficit: an unsolved issue, Revista
831 Brasil. Agrociên., 9 (4), 317–322, 2003.

832 Tuzet, A., Perrier, A., and Leuning, R.: A coupled model of stomatal conductance,
833 photosynthesis and transpiration, Pl. Cell Environ., 26, 1097–1116, 2003.

834 van der Tol, C., van der Tol, S., Verhoef, A., Su, B., Timmermans, J., Houldcroft, C., and
835 Gieske, A.: A Bayesian approach to estimate sensible and latent heat over vegetated land
836 surface, Hydrol. Earth Sys. Sci., 13, 749–758, doi:10.5194/hess-13-749-2009, 2009.

837 Venturini, V., Islam, S., and Rodriguez, L.: Estimation of evaporative fraction and
838 evapotranspiration from MODIS products using a complementary based model, Remote
839 Sens. Environ., 112(1), 132-141, 2008.

840 von Randow, R.C.S., von Randow, C., Hutjes, R.W.A., Tomasella, J., and Kruijt, B.:
841 Evapotranspiration of deforested areas in central and southwestern Amazonia, Theor.
842 Appl. Climatol., 109:205–220, doi: 10.1007/s00704-011-0570-1, 2012.

Hydrol. Earth Syst. Sci. Discuss., doi:10.5194/hess-2015-552, 2016
Manuscript under review for journal Hydrol. Earth Syst. Sci.
Published: 27 January 2016

843 Villagarcía, L., Were, A., García, M., and Domingo, F.: Sensitivity of a clumped model of
844 evapotranspiration to surface resistance parameterisations: Application in a semi-arid
845 environment, Agric. For. Meteorol., 150 (7), 1065-1078, 2010.

846
847
848
849
850
851
852
853
854
855
856
857
858
859
860
861
862
863
864
865

Hydrol. Earth Syst. Sci. Discuss., doi:10.5194/hess-2015-552, 2016
Manuscript under review for journal Hydrol. Earth Syst. Sci.
Published: 27 January 2016

Hydrology and Earth System Sciences
Discussions

866 **Table 1**. Overview of the LBA tower sites.

Biome	PFT	Site	LBA Code	Data availability period	Latitude	Longitude	Tower height (m)	Annual rainfall (mm)
Forest	Tropical rainforest (TRF)	Manaus KM34	K34	06/1999 to 09/2006	-2.609	-60.209	50	2329
Forest	Tropical moist forest (TMF)	Santarem KM67	K67	01/2002 to 01/2006	-2.857	-54.959	63	1597
Forest	Tropical moist forest (TMF)	Santarem KM83	K83	07/2000 to 12/2004	-3.018	-54.971	64	1656
Forest	Tropical dry forest (TDF)	Reserva Biológica Jarú	RJA	03/1999 to 10/2002	-10.083	-61.931	60	2354
Pasture	Pasture (PAS)	Santarem KM77	K77	01/2000 to 12/2001	-3.012	-54.536	18	1597
Pasture	Pasture (PAS)	Fazenda Nossa Senhora	FNS	03/1999 to 10/2002	-10.762	-62.357	8.5	1743

867

868

869 **Table 2**. Comparative statistics for the STIC and tower-derived hourly g_A and g_C for a range of PFTs
870 in the Amazon Basin (LBA tower sites). Values in parenthesis are ± one standard deviation (standard
871 error for correlation).

PFTs	$g_{A\text{-}STIC}$ vs. $g_{A\text{-}BM13}$					$g_{C\text{-}STIC}$ vs. $g_{C\text{-}INV}$			
	RMSD (m s^{-1})	R^2	Slope	Offset (m s^{-1})	N	RMSD (m s^{-1})	R^2	Slope	Offset (m s^{-1})
TRF	0.013	0.41 (±0.03)	1.07 (±0.047)	0.0031 (±0.0008)	1159	0.012	0.14 (±0.04)	0.39 (±0.039)	0.0097 (±0.0007)
TMF	0.012	0.55 (±0.12)	0.81 (±0.023)	0.0006 (±0.0006)	1927	0.009	0.55 (±0.12)	0.85 (±0.025)	0.0032 (±0.0005)
TDF	0.007	0.49 (±0.15)	0.89 (±0.041)	0.0019 (±0.0006)	787	0.012	0.33 (±0.19)	0.30 (±0.022)	0.0050 (±0.0005)
PAS	0.012	0.22 (±0.18)	1.03 (±0.083)	0.0059 (±0.0007)	288	0.007	0.58 (±0.12)	0.65 (±0.025)	0.0024 (±0.0003)
Mean	**0.012**	**0.44 (±0.10)**	**0.76 (±0.016)**	**0.0047** (±0.003)	**4161**	**0.010**	**0.39 (±0.08)**	**0.63 (±0.016)**	**0.0046 (±0.0003)**

872 N = number of data points; RMSD = root mean square deviation between predicted (P) and observed (O)
873 variables = $\left[\frac{1}{N}\sum_{i=0}^{N}(P_i - O_i)^2\right]^2$.

874

875

876

Hydrol. Earth Syst. Sci. Discuss., doi:10.5194/hess-2015-552, 2016
Manuscript under review for journal Hydrol. Earth Syst. Sci.
Published: 27 January 2016

Hydrology and Earth System Sciences
Discussions
Open Access
EGU

877 **Table 3**. Comparative statistics for the STIC and tower-derived hourly λE and H for a range of PFTs
878 in the Amazon Basin (LBA tower sites). Values in parenthesis are ±one standard deviation (standard
879 error for correlation).

PFTs	*λE*				H				
	RMSD (W m^{-2})	R^2	Slope	Offset (W m^{-2})	RMSD (W m^{-2})	R^2	Slope	Offset (W m^{-2})	N
TRF	28	0.96 (±0.007)	1.10 (±0.008)	-16 (±2)	34	0.52 (±0.030)	0.60 (±0.025)	29 (±2)	1159
TMF	20	0.98 (±0.004)	1.08 (±0.004)	-11 (±1)	23	0.71 (±0.019)	0.61 (±0.014)	20 (±1)	1927
TDF	26	0.96 (±0.009)	0.96 (±0.008)	-7 (±2)	30	0.66 (±0.032)	0.89 (±0.035)	20 (±3)	787
PAS	31	0.96 (±0.009)	1.14 (±0.010)	-2 (±2)	33	0.88 (±0.016)	0.67 (±0.011)	9 (±1)	288
Mean	**33**	**0.94 (±0.005)**	**1.04 (±0.005)**	**-1 (±1)**	**37**	**0.61 (±0.021)**	**0.58 (±0.009)**	**24 (±2)**	**4161**

880
881
882
883
884
885
886
887
888
889
890
891
892
893
894
895

Hydrol. Earth Syst. Sci. Discuss., doi:10.5194/hess-2015-552, 2016
Manuscript under review for journal Hydrol. Earth Syst. Sci.
Published: 27 January 2016

Hydrology and Earth System Sciences
Discussions

Figure 1. Examples of monthly averages of the diurnal time series of canopy-scale (a) g_A and (b) g_C estimated for two different biomes (forest and pasture) in the Amazon Basin (LBA sites K34 and FNS). The time series of four different g_A estimates and their corresponding g_C estimates are shown here.

(a) Time series g_A

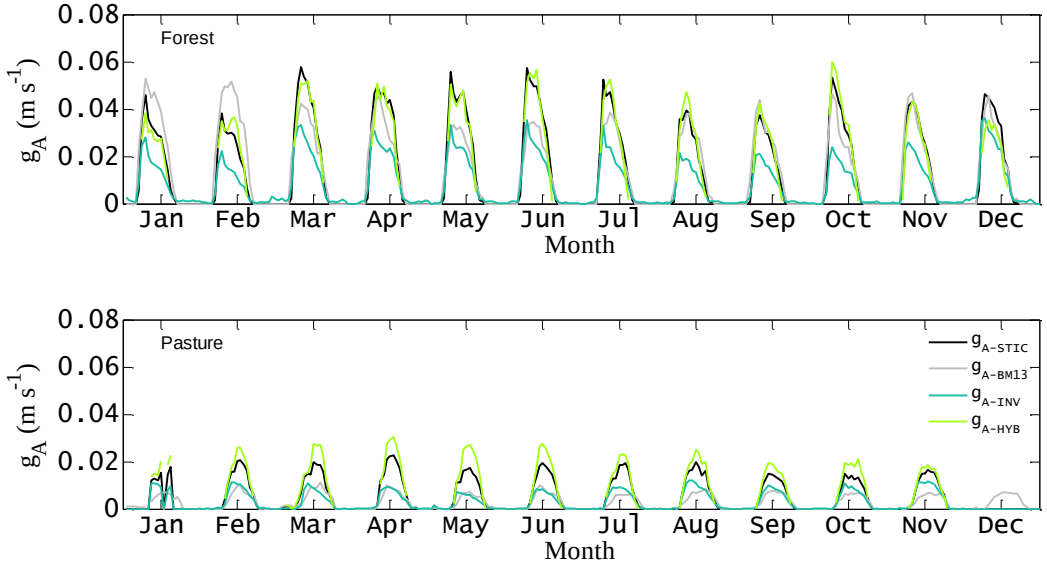

(b) Time series g_C

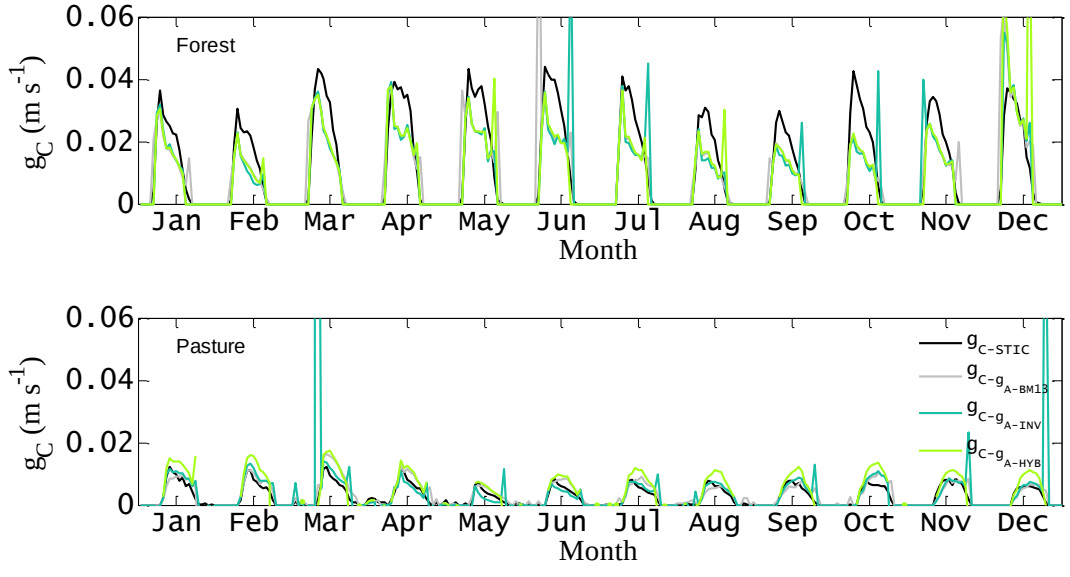

Hydrol. Earth Syst. Sci. Discuss., doi:10.5194/hess-2015-552, 2016
Manuscript under review for journal Hydrol. Earth Syst. Sci.
Published: 27 January 2016

Hydrology and Earth System Sciences
Discussions

Figure 2. (a) Comparison between STIC derived g_A ($g_{A\text{-}STIC}$) with an estimated aerodynamic conductance based on friction velocity (u^*) and wind speed (u) according to Baldocchi and Ma (2013) ($g_{A\text{-}BM13}$), (b) Comparison between $g_{A\text{-}STIC}$ with an inverted g_A ($g_{A\text{-}INV}$) based on EC observations of λE and D_A, (c) Comparison between $g_{A\text{-}STIC}$ with a hybrid g_A ($g_{A\text{-}HYB}$) based on EC observations of H and estimated T_0 over the LBA EC sites, (d) Comparison between residual g_A differences versus u and u^*, (e) and (f) Relationship between wind and shear derived g_A versus ϕ, T_R, and D_A over the LBA EC sites.

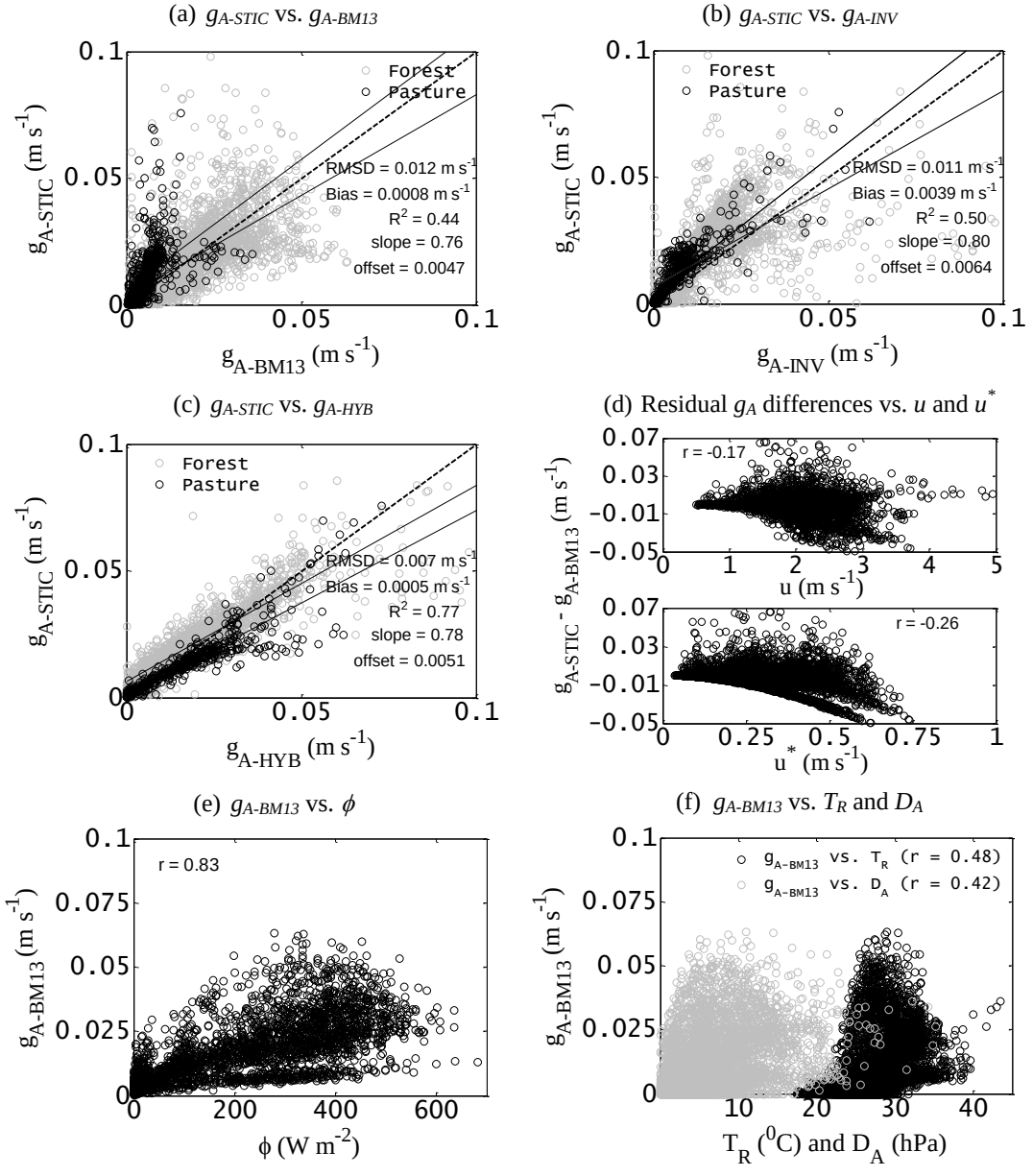

Hydrol. Earth Syst. Sci. Discuss., doi:10.5194/hess-2015-552, 2016
Manuscript under review for journal Hydrol. Earth Syst. Sci.
Published: 27 January 2016

909 **Figure 3**. (a) comparison between STIC derived g_C ($g_{C\text{-}STIC}$) and g_C computed by inverting the PM
910 model ($g_{C\text{-}INV}$) over the LBA EC sites, where $g_{A\text{-}BM13}$ was used as aerodynamic input in conjunction
911 with tower measurements of λE, radiation and meteorological variables, (b) Residual g_C differences
912 versus wind speed (u) and friction velocity (u^*) over the LBA EC sites.

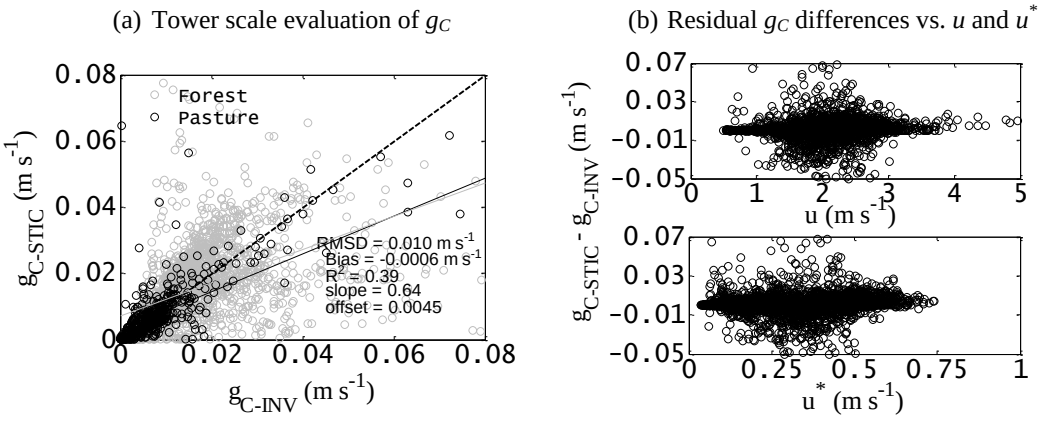

913
914
915
916
917
918
919
920
921
922
923
924
925
926
927
928
929

Hydrol. Earth Syst. Sci. Discuss., doi:10.5194/hess-2015-552, 2016
Manuscript under review for journal Hydrol. Earth Syst. Sci.
Published: 27 January 2016

Hydrology and Earth System Sciences
Discussions
Open Access
EGU

930 **Figure 4**. Comparison between STIC derived (a) λE and (b) H over four different PFTs in the
931 Amazon Basin (LBA tower sites). MAPD is the percent error defined as the mean-absolute-deviation
932 between predicted and observed variable divided by mean observed variable.

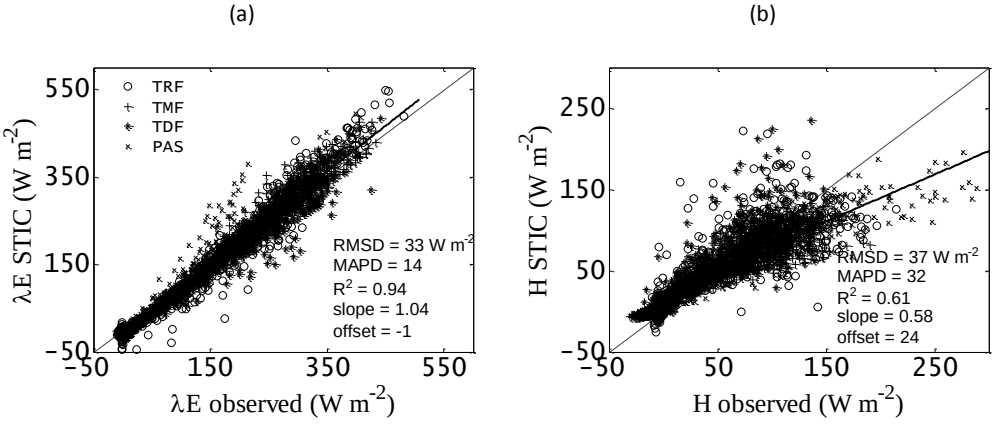

933
934
935
936
937
938
939
940
941
942
943
944
945
946
947
948
949

Hydrol. Earth Syst. Sci. Discuss., doi:10.5194/hess-2015-552, 2016
Manuscript under review for journal Hydrol. Earth Syst. Sci.
Published: 27 January 2016

Hydrology and Earth System Sciences
Discussions

Figure 5. Correlation of coupling (1-Ω) with (a) transpiration (λE_T) and (b) evaporation (λE_E) and over four different PFTs by combining data for all the years, only during dry seasons for all the years, and during drought year 2005. Data for 2005 was not available for TDF and PAS. (c) to (e) Examples of diurnal pattern of Ω (black lines), λE_E (grey dotted lines) and λE_T (grey solid lines) estimated over two ecohydrologically contrasting biomes (K34 for forest and FNS for pasture) in the Amazon Basin (LBA tower sites) during wet and dry seasons.

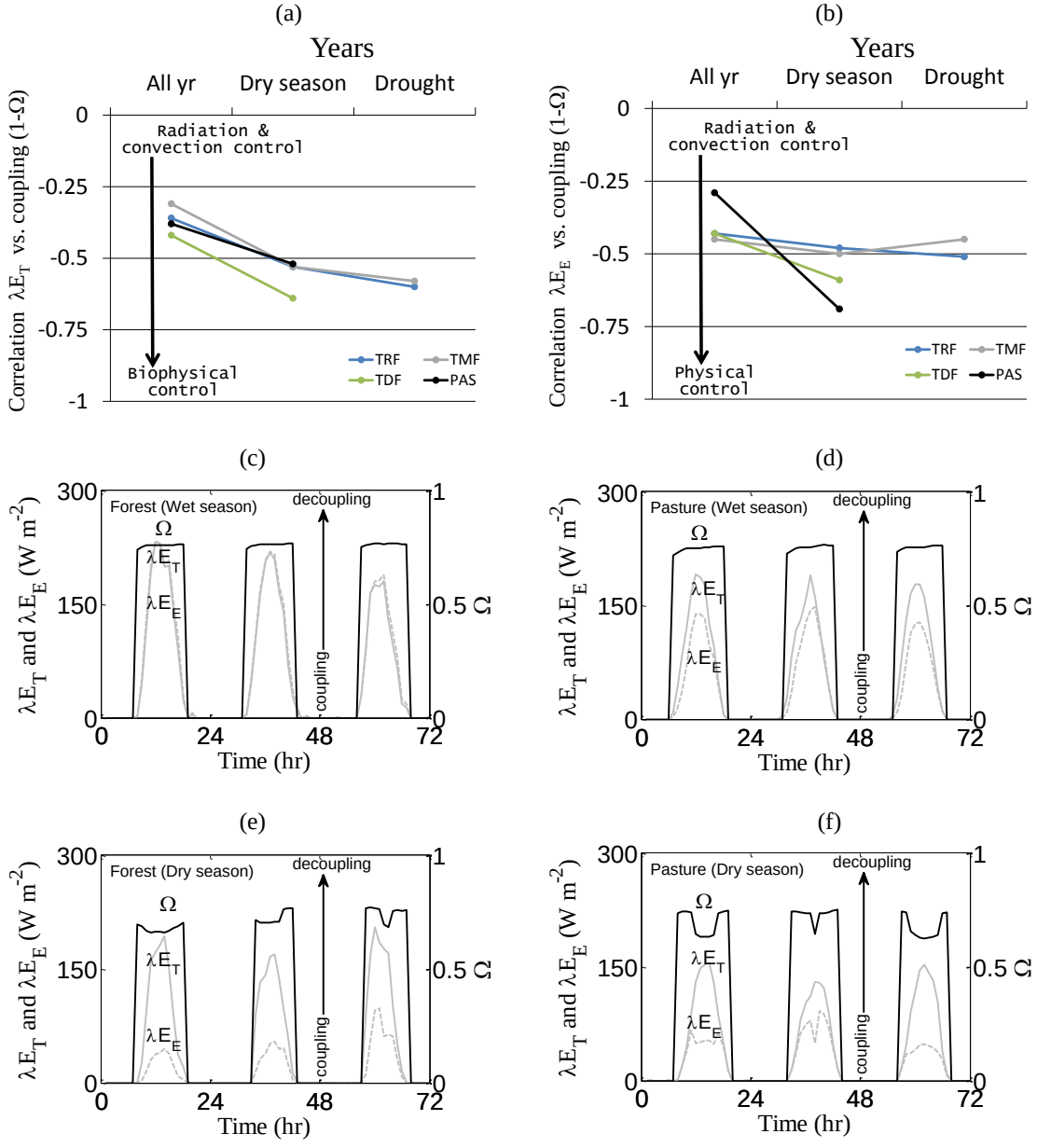

Hydrol. Earth Syst. Sci. Discuss., doi:10.5194/hess-2015-552, 2016
Manuscript under review for journal Hydrol. Earth Syst. Sci.
Published: 27 January 2016

957 **Figure 6**. Scatter plots of transpiration (λE_T) and evaporation (λE_E) versus g_C and g_A over four
958 different PFTs in the Amazon Basin (LBA tower sites).

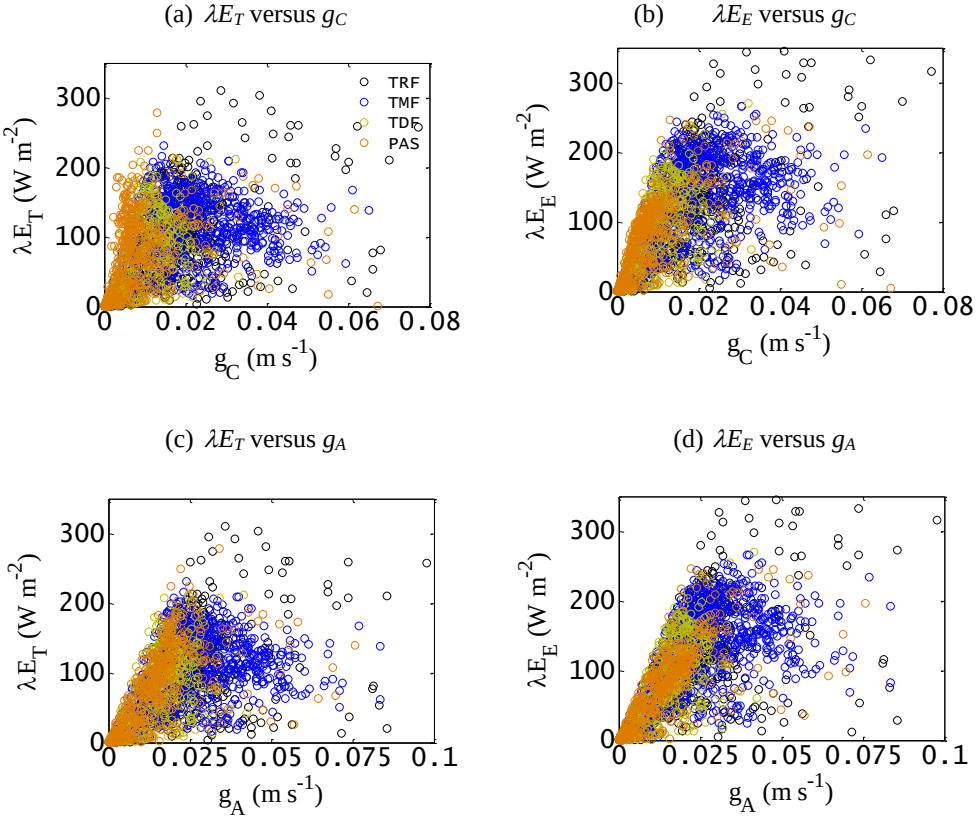

959
960
961
962
963
964
965
966
967
968

Hydrol. Earth Syst. Sci. Discuss., doi:10.5194/hess-2015-552, 2016
Manuscript under review for journal Hydrol. Earth Syst. Sci.
Published: 27 January 2016

Hydrology and Earth System Sciences
Discussions

Figure 7. Illustrative examples of the occurrence of diurnal hysteresis of transpiration (λE_T) during wet and dry seasons with canopy and environmental controls over two different sites with different annual rainfall (2329 mm and 1597 mm, respectively) in the Amazon Basin (LBA tower sites K34 and FNS).

(a) Rainforest: Wet season

(b) Pasture: Wet season

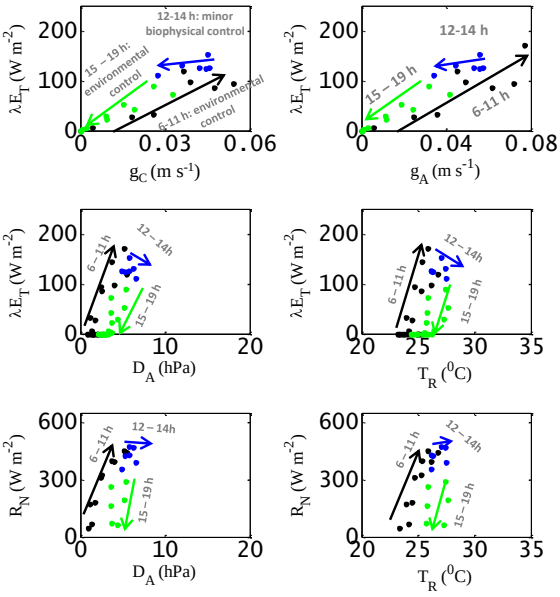

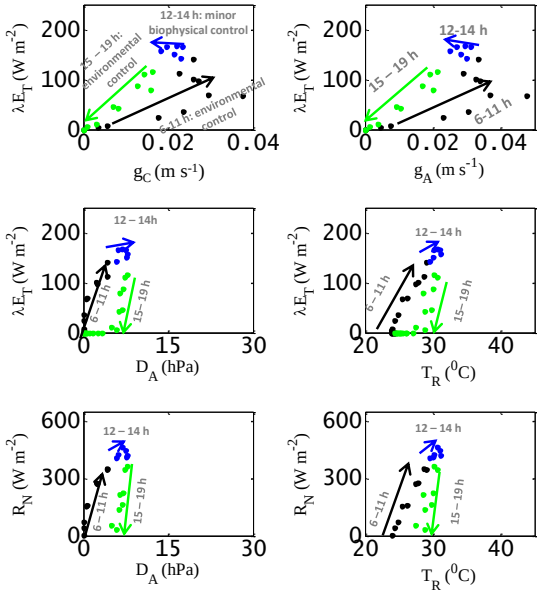

(c) Rainforest: Dry season

(d) Pasture: Dry season

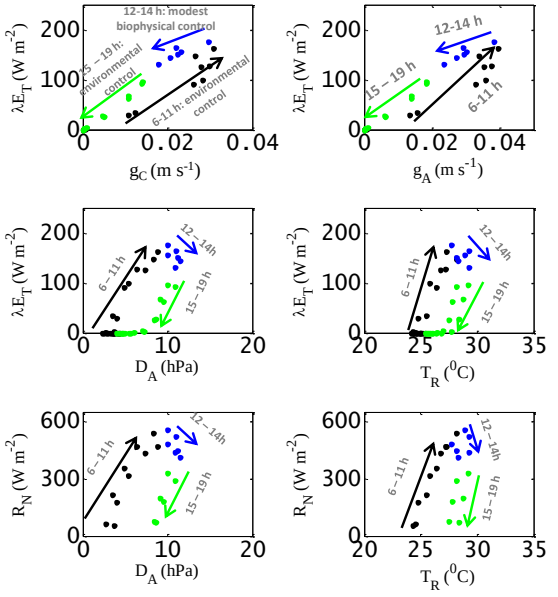

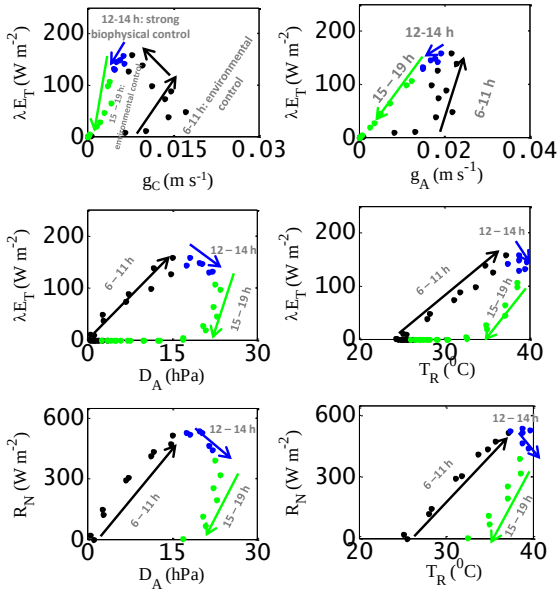

Hydrol. Earth Syst. Sci. Discuss., doi:10.5194/hess-2015-552, 2016
Manuscript under review for journal Hydrol. Earth Syst. Sci.
Published: 27 January 2016

Hydrology and Earth System Sciences
Discussions

Figure 8. (a) Response of retrieved g_C to atmospheric vapor pressure deficit (D_A) for different classes of net radiation (R_N), (b) Response of retrieved g_C to transpiration for different classes of D_A, (c) Response of retrieved g_C to radiometric surface temperature (T_R) for different classes D_A, (d) Relationship between retrieved g_A and radiometric surface temperature and air temperature difference (T_R - T_A) in the Amazon Basin (LBA tower sites).

(a) g_C versus D_A

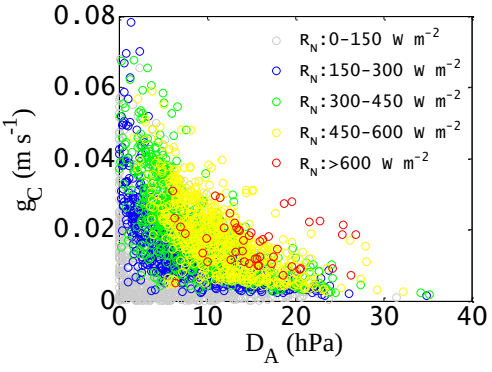

(b) g_C versus λE_T

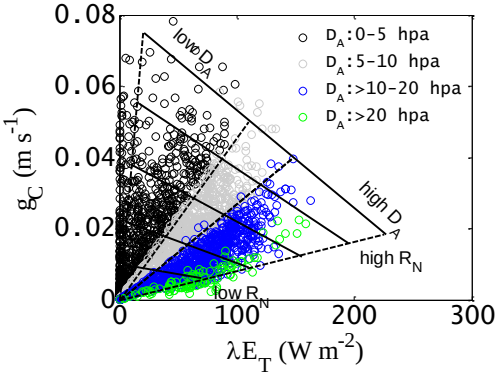

(c) g_C versus T_R

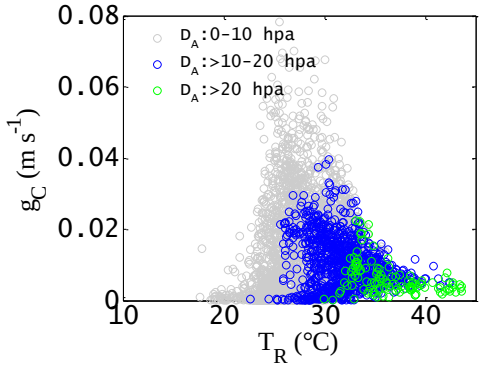

(d) g_A versus $T_R - T_A$

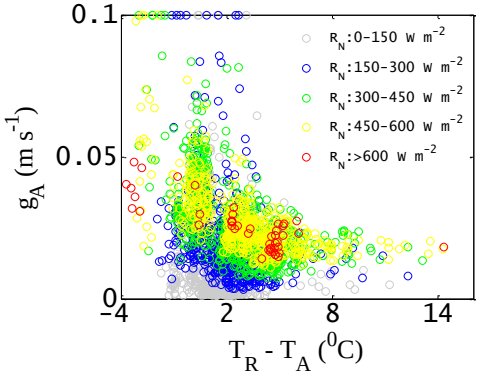

Hydrol. Earth Syst. Sci. Discuss., doi:10.5194/hess-2015-552, 2016
Manuscript under review for journal Hydrol. Earth Syst. Sci.
Published: 27 January 2016

Hydrology and Earth System Sciences
Discussions
Open Access
EGU

Figure 9. (a) Scatter plots between source-sink height (or in-canopy) vapor pressure deficit (D_0) and atmospheric vapor pressure deficit (D_A) for two different classes of g_C/g_A ratios over four PFTs, which clearly depicts a strong coupling between D_0 and D_A for low g_C/g_A ratios. (b) Histogram distribution of g_C/g_A ratios over the four PFTs in the Amazon Basin (LBA tower sites). (c) Scatter plots between g_C/g_A ratio versus surface air temperature difference (T_R - T_A) for the four PFT during wet season and dry season in the Amazon Basin (LBA tower sites).

(a) D_0 vs. D_A over four PFTs

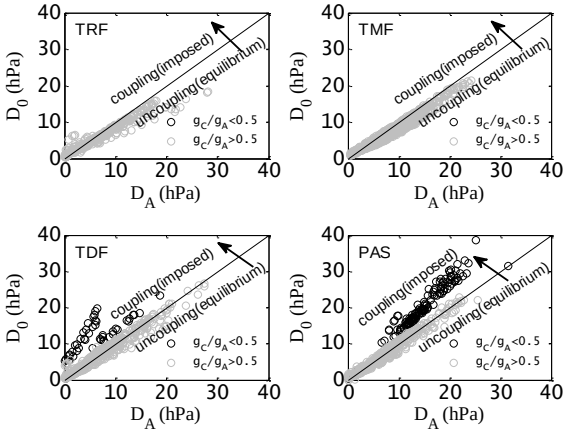

(b) Distribution of g_C/g_A ratio over four PFTs

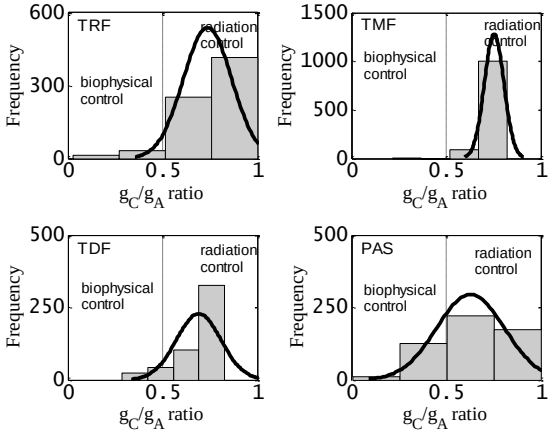

(c) g_C/g_A vs. T_R-T_A over four PFTs

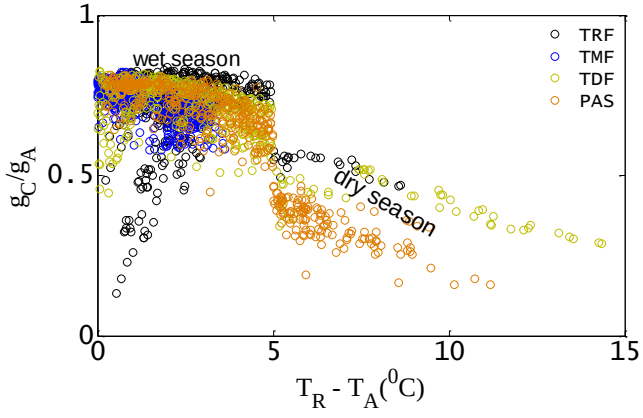

Hydrol. Earth Syst. Sci. Discuss., doi:10.5194/hess-2015-552, 2016
Manuscript under review for journal Hydrol. Earth Syst. Sci.
Published: 27 January 2016

Figure A1. Schematic representation of one-dimensional description of STIC (v 1.2). In the STIC1.2, a feedback is established between the surface layer evaporative fluxes and source/sink height mixing and coupling, and the connection is shown in dotted arrows between e_0, e_0^*, g_A, g_C, and λE. Here, r_A and r_C are the aerodynamic and canopy (or surface in case of partial vegetation cover) resistances, g_A and g_C are the aerodynamic and canopy conductances (reciprocal of resistances), e_S^* is the saturation vapor pressure of the surface, e_0^* is the saturation vapor pressure at the source-sink height, T_0 is the source-sink height temperature (i.e. aerodynamic temperature) that is responsible for transferring the sensible heat (H), e_0 is the source-sink height vapor pressure, e_S is the vapor pressure at the surface, z_0 is the roughness length, T_R is the radiometric surface temperature, T_{SD} is the source-sink height dewpoint temperature, M is the surface moisture availability or evaporation coefficient, R_N and G are net radiation and ground heat flux, T_A, e_A, and D_A are temperature, vapor pressure, and vapor pressure deficit at the reference height (z_R), λE is the latent heat flux, H is the sensible heat flux, respectively.

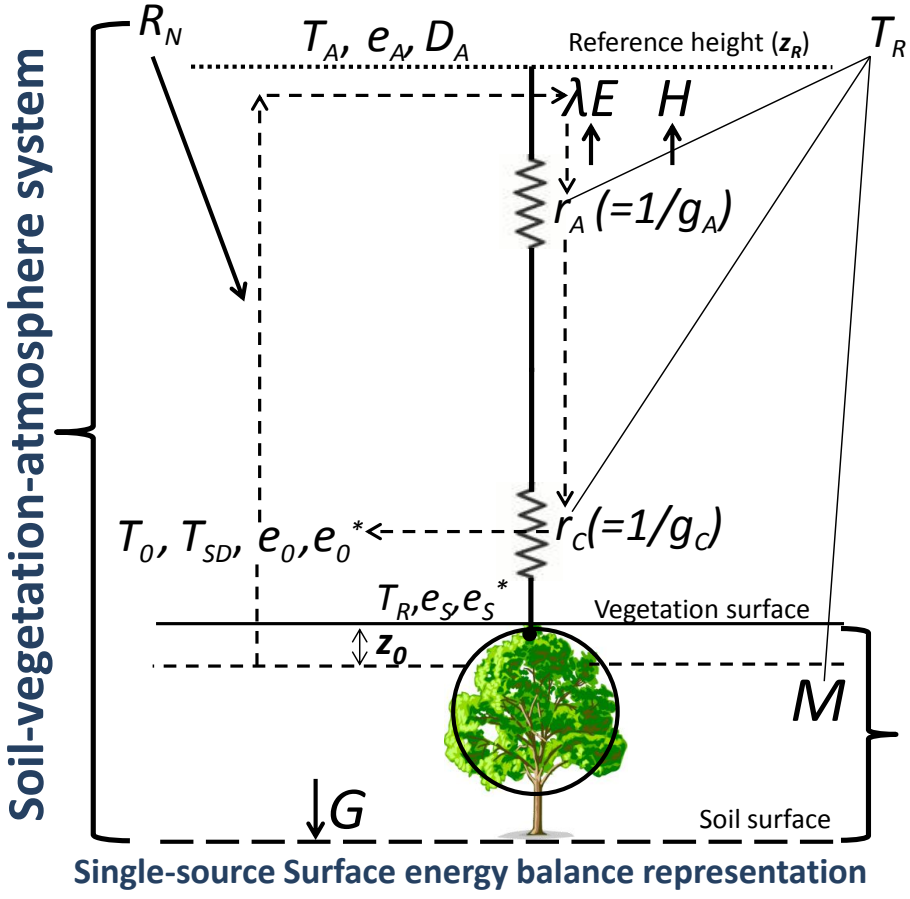

Hydrol. Earth Syst. Sci. Discuss., doi:10.5194/hess-2015-552, 2016
Manuscript under review for journal Hydrol. Earth Syst. Sci.
Published: 27 January 2016

Hydrology and Earth System Sciences
Discussions

Figure A2. (a) Convergence of the iteration method for retrieving the source/sink height (or in-canopy) vapor pressures (e_0 and D_0) and Priestley-Taylor coefficient (α). (b) Convergence of the iteration method for retrieving the surface wetness (M) and source/sink height dewpoint temperature (T_{SD}). The initial values of g_A, g_C, and T_0 were determined with α = 1.26. The process is then iterated by updating e_0, D_0, M, T_{SD}, and α in subsequent iterations with the previous estimates of g_A, g_C, and T_0.